Acta Pharmaceutica Sinica B 2026;16(8):5086−5107

Chinese Pharmaceutical Association
Institute of Materia Medica, Chinese Academy of Medical Sciences

Acta Pharmaceutica Sinica B

www.elsevier.com/locate/apsb
www.sciencedirect.com

ORIGINAL ARTICLE

Progranulin drives acetaminophen-induced acute liver injury by limiting hepatic recruitment of eosinophils *via* suppressing interleukin-33 expression

Yin Tang[a,†], Siyuan Xie[a,†], Yueyue He[a,†], Jiayu Liu[a], Mingang Pan[a], Renlin Yu[a], Linghong Zhou[a], Mengxue Liu[a], Yi Liu[b], Ju Cao[a,*]

[a]*Department of Laboratory Medicine, The First Affiliated Hospital of Chongqing Medical University, Chongqing 400016, China*
[b]*Department of Surgery, School of Medicine, Stanford University, Stanford, CA 94305, USA*

Received 30 September 2025; received in revised form 8 December 2025; accepted 11 December 2025

KEY WORDS

Acetaminophen;
Acute liver injury;
Eosinophils;
Interleukin-33;
Progranulin;
Liver sinusoidal endothelial cells;
AMP-Activated protein kinase;
Forkhead box O3

Abstract Drug-induced liver injury (DILI), particularly acetaminophen (APAP)-induced acute liver injury (ALI), is the leading cause of acute liver failure. Progranulin (PGRN) is a multifunctional glycoprotein. However, the role of PGRN in APAP-induced ALI remains unknown. Here, we found that PGRN serum concentration increased and correlated with disease severity in the patients with APAP overdose. Mice with PGRN deficiency were protected from APAP-induced ALI or concanavalin A (ConA)-induced ALI. They exhibited substantially increased hepatic recruitment of eosinophils, which depended on up-regulated IL-33 that was primarily released from liver sinusoidal endothelial cells (LSECs). Moreover, treatment of mice with blocking PGRN antibody could prophylactically and therapeutically treat APAP- or ConA-induced ALI, while injection of recombinant PGRN protein enhanced APAP-induced liver damage and worsened survival. Mechanistically, PGRN inhibited APAP-induced IL-33 expression in LSECs by dampening the activation of AMP-activated protein kinase (AMPK)-forkhead box O3 (FOXO3) signaling pathway. Therefore, PGRN should be considered as a new biomarker and potential therapeutic target to treat DILI.

*Corresponding author.
E-mail address: caoju723@163.com (Ju Cao).
[†]These authors made equal contributions to this work.
Peer review under the responsibility of Chinese Pharmaceutical Association and Institute of Materia Medica, Chinese Academy of Medical Sciences.

https://doi.org/10.1016/j.apsb.2026.02.011

1. Introduction

Drug-induced liver injury (DILI) is a global primary health issue because it is the most common cause of acute liver failure GSH and one of the main reasons for the termination of drug development[1,2]. Acetaminophen (APAP), a widely used analgesic and antipyretic over-the-counter medicine worldwide, is the leading individual cause of DILI, responsible for nearly 50% of all acute liver failure cases in the United States[3]. Hepatotoxicity caused by APAP is the archetypal model of DILI and probably the most relevant to human DILI, which can be modelled in rodents after administration of an acute or cumulative overdose[4]. The mechanism for APAP toxicity begins with its reactive metabolite, *N*-acetyl-*p*-benzoquinone imine, which rapidly depletes glutathione (GSH), causes hepatocyte necrosis. Hepatocyte death subsequently activates Kupffer cells to release cytokines and chemokines, which drive hepatic infiltration of peripheral immune cells, triggering sterile inflammation and aggravating liver injury[5,6]. Currently, *N*-acetylcysteine is the only approved treatment for APAP-overdose patients. However, *N*-acetylcysteine intervention is effective only when administered within 24 h of APAP overdose and is less effective in late-presenting patients[7]. Therefore, it is imperative to further elucidate the underlying mechanisms of APAP-induced acute liver injury (ALI), especially endogenous detrimental or beneficial pathways that can expand on therapeutic options.

Progranulin (PGRN), a multifunctional growth factor-like protein expressed by a variety of cell types and secreted broadly, serves an important function in the physiologic and pathologic processes[8,9]. There is a consensus that aberrant PGRN expression is linked to disease[10,11]. Our group has shown that elevated circulating level of PGRN was associated with disease severity in human patients with candidemia and influenza virus infection[12,13], and PGRN aggravated immunopathology of *Candida albicans* and influenza virus infection in mice[13,14]. However, PGRN played a protective role in host defense during bacterial infection[15-17]. There is emerging evidence that PGRN expression is associated with liver diseases[18,19]. It has been demonstrated that serum PGRN acted as an independent predictor of the extent of liver fibrosis in nonalcoholic fatty liver disease patients[20]. Furthermore, in two different models of chronic liver disease, including methionine-choline-deficient diet-induced nonalcoholic steatohepatitis and carbon tetrachloride (CCl_4)-induced liver fibrosis, PGRN showed protective effects against hepatic injury[21]. However, little is known about the role of PGRN in DILI. Here, we present unexpected findings revealing that PGRN drives progression of APAP-induced ALI by negatively regulating hepatic recruitment of eosinophils through suppressing IL-33 production from liver sinusoidal endothelial cells (LSECs), which may serve as a biomarker and therapeutic target to combat DILI.

2. Materials and methods

2.1. Human samples

Peripheral blood samples were obtained from 62 patients with APAP overdose at the First Affiliated Hospital of Chongqing Medical University (Supporting Information Table S1). APAP overdose as a diagnosis was made by a physician based on standard clinical criteria, including reported history of APAP overdose, detectable serum APAP levels, and increased ALT and AST levels. All patients received standard therapy with *N*-acetylcysteine. Blood samples were collected in heparinized collection tubes at the time of study admission by hospital staff. Serum was prepared within 2 h of blood collection by centrifugation at $1200\times g$ for 15 min at 20 °C, and then was stored at −80 °C. A second set of 103 patients with DILI (caused by traditional Chinese Medicine, Sulfasalazine, Cefotiam, Fenbid, Cetirizine, Azathioprine, Amoxycillin, or anti-tumor drugs) was also obtained from the First Affiliated Hospital of Chongqing Medical University (Supporting Information Table S2). Healthy control volunteers were recruited in this study from the Physical Examination Center of the First Affiliated Hospital of Chongqing Medical University. This study involves human participants and was approved by the Ethics Committee of The First Affiliated Hospital of Chongqing Medical University (Registration numbers: 2021-187 and 2021-655). No informed consent was needed, as this study was non-interventional, and complementary blood samples were obtained during patients' routine blood sampling after completion of routine follow-up tests. Nevertheless, non-opposition to inclusion in the protocol was recorded from every patient or the patient's next of kin.

2.2. Animals

Wild-type (WT) C57BL/6J mice were procured from Tengxin Company (Beijing, China). PGRN knockout (PGRN KO) mice, bred on a C57BL/6J background, were sourced from the Jackson Laboratory (Bar Harbor, ME). Their littermates were used as the control group. Myeloid-specific PGRN conditional KO mice, also bred on a C57BL/6J background, were acquired from Cyagen Biosciences (Suzhou, China). $Grn^{flox/flox}$ mice were generated using the CRISPR-Cas9 system. *Lyz2-Cre*$^{+}$-$Grn^{flox/flox}$ (PGRN$^{f/f}$ Cre $^{+}$ mice) mice were generated by crossing the *Lyz2-Cre*$^{+}$ mice with $Grn^{flox/flox}$ mice for specific deletion of PGRN in myeloid cells, and their *Lyz2-Cre*$^{-}$-$Grn^{flox/flox}$ (PGRN$^{f/f}$ Cre^{-} mice) littermates were used as controls. Mouse genotypes were determined by PCR using genomic tail DNA. Sequences of primers used for amplification of DNA by PCR are listed in Supporting Information Table S3. Sex- and age-matched mice [age, 6−8 weeks; weight, 20−22 g] were used in all experiments. All mice were maintained in a specific pathogen-free facility. Throughout the experiment, the mice were maintained under a 12-h light/dark cycle. The study adhered to the Guidelines for the Care and Use of Experimental Animals. The experimental protocol involving animals received approval from the Animal Ethics Committee of Chongqing Medical University (approval number: IACUC-CQMU-2023-09065).

2.3. Bone marrow (BM)-chimeric mice

Bone marrow (BM) transplantation experiments were performed as described previously[14,22]. Six-week-old recipient mice (PGRN

KO mice or wild type littermates) were exposed to 8.5 Gy irradiation to destroy their own BM 2.5 h before transplantation of BM cells from donors. Donor BM cells were extracted from donor mice (PGRN KO mice or WT littermates) by flushing the femur and tibia bones with phosphate-buffered saline (PBS). Each recipient mouse was injected with 1×10^7 BM cells (in 200 μL PBS) through the tail vein, and was given antibiotics in drinking water with 100 mg/L levofloxacin and 200 mg/L metronidazole in the following two weeks. Chimaeras were then used for subsequent experiments at 8 weeks after the initial reconstitution.

2.4. Animal experiments

For APAP administration, mice were fasted overnight (5:00 PM to 9:00 AM) before being injected intraperitoneally (i.p.) with APAP (20 mg/mL, A7085, Sigma−Aldrich), which was prepared in warm PBS. APAP was administered at a dosage of 500−750 mg/kg for survival analysis. For hepatic toxicity assessment, the dose of APAP administered to male mice was 300 mg/kg, while the dose given to female mice was 400 mg/kg[23-25]. During survival analysis, the mice were monitored, and their survival status was documented every 12 h post-APAP injection, with the analysis concluding after 72 h. To assess hepatic toxicity, blood and liver samples were collected at the indicated time points for further biochemical, immunological, and histological analysis. Throughout the study, all possible measures were taken to minimize distress in the mice.

For recombinant murine PGRN protein (rmPGRN) treatment, mice were i.p. injected with rmPGRN (2 μg/mouse, 2557-PG, R&D Systems) or vehicle at 1 h prior to APAP treatment. For rmIL-33 treatment, mice were i.p. injected with rmIL-33 (500 ng/mouse, 580,504, Biolegend) or vehicle at 1 h prior to APAP treatment, followed by injection i.p. with rmPGRN (2 μg/mouse) or vehicle at 30 min prior to APAP treatment.

For PGRN neutralization, mice were i.p. injected with anti-mouse PGRN antibody (1 μg/mouse, AF2557, R&D systems) at 12 h and 1 h prior to APAP treatment, or with 2 μg/mouse at the time of or 1 h after APAP treatment. For IL-33 neutralization, mice were i.p. injected with anti-mouse IL-33 antibody (1 μg/mouse, AF3626, R&D Systems) at 12 and 1 h prior to APAP treatment. For eosinophil depletion, mice were injected i.p. with anti-mouse Siglec-F antibody (10 μg/mouse, MAB17061, R&D Systems) 24 h before APAP injection. Control mice were injected with IgG. For macrophage depletion, WT mice were injected i.p. with 200 μL Clodronate-liposomes (40337ES08, YEASEN, Shanghai, China) or 200 μL PBS-liposomes (40338ES08, YEASEN, Shanghai, China) 24 h before APAP injection. For neutrophil depletion, WT mice were injected i.p. with 100 μg anti-mouse Ly-6G antibody (BE0075-1, Bio X cell) 24 h before APAP injection. The control mice were injected with an equivalent amount of rat IgG (BP0089, Bio X cell).

For AMP-activated protein kinase (AMPK) inhibitor treatment, mice were injected i.p. with Compound C (Dorsomorphin 2HCl, S7306, Selleck, 10 mg/kg) or vehicle (sterile saline) at 30 min prior to APAP treatment.

2.5. Mice ConA liver injury model

For the concanavalin A (ConA)-induced liver injury model, mice were intravenously injected *via* the tail vein of ConA (C2010, Sigma) at sublethal doses of 10 mg/kg body weight, and were subsequently sacrificed at 24 h following ConA administration. Survival testing was performed with ConA at a lethal dose of 20 mg/kg.

To evaluate the therapeutic potential of PGRN inhibition, a PGRN-neutralizing antibody (2 μg/mouse) was reconstituted in sterile PBS and administered to WT mice immediately after, at 1 h after, and at 2 h after ConA treatment.

2.6. Histopathology

Liver tissues were fixed in 4% paraformaldehyde. Paraffin-embedded sections, each with a thickness of 5 μm, were used for hematoxylin and eosin (H&E) staining to examine necrotic areas and terminal deoxynucleotidyl transferase-mediated dUTP nick end labeling (TUNEL) staining to assess cell apoptosis. H&E and TUNEL staining of these sections were conducted using the H&E Staining Kit (Solarbio, China) and the TUNEL Apoptosis Assay Kit (Roche, Mannheim, Germany) according to the manufacturers' instructions. Images were captured under a light microscope (Olympus, Tokyo, Japan). The necrosis areas were outlined according to the cellular structure and color. The percentages of necrosis areas were averaged from 5 to 7 random view fields of each section (× 100 magnification) using ImageJ software. TUNEL-positive cells were defined as those showing strong nuclear staining that was co-localized with DAPI-stained nuclei. The relative number of TUNEL-positive cells was also counted under the ImageJ software.

2.7. Immunofluorescence

The expression of EMBP (sc-365,701, Santa Cruz Biotechnologies, Santa Cruz, CA, USA) and forkhead box O3 (FOXO3) (66428-1-Ig, Proteintech, Wuhan, China) was detected using immunofluorescence. The sections and cells were permeabilized with 0.5% Triton X-100 and then blocked with 30% goat serum (C0265, Beyotime Biotechnology, Shanghai, China) for 30 min at room temperature, and subsequently incubated with primary antibodies overnight at 4 °C. Afterwards, they were incubated with a fluorescent secondary antibody and analyzed using Nikon AXR NSPARC laser confocal microscope (Nikon, Tokyo, Japan).

2.8. Measurements of transaminase activities, CYP2E1 activity, GSH, and cytokine levels

Enzyme-linked immunosorbent assay (ELISA) kits for the measurement of human PGRN (DY2420), mouse PGRN (DY2557), mouse CXCL1 (DY453), mouse CCL2 (DY479), mouse TNF-α (DY410), mouse IFN-γ (DY485), mouse IL-1β (DY401), mouse IL-6 (DY406), mouse IL-4 (DY404), mouse IL-13 (DY413), and mouse IL-33 (DY3626) were purchased from R&D Systems. CYP2E1 was measured by using the mouse Cytochrome P450 2E1 (CYP2E1) ELISA kit (CSB-EL006425MO, CUSABIO, Wuhan, China). CYP2E1 activity levels were measured by the rate of *p*-nitrophenol (PNP) oxidation to *p*-nitrocatechol, as described[26,27]. The activities of alanine aminotransferase (ALT) and aspartate aminotransferase (AST) were measured by using the ALT and AST assay kits (C009-2 and C010-2, Nanjing Jiancheng, China). Glutathione (GSH) levels were measured using a GSH assay kit (BC1175, Solarbio, China). All measurements were performed according to the manufacturer's protocols.

2.9. RNA sequencing (RNA-seq)

After modeling, liver tissue samples were collected 24 h later. These samples were placed in sample cryovials, rapidly frozen in

liquid nitrogen, and then stored at −80 °C in a low-temperature refrigerator. Total RNA was extracted from liver tissues using Trizol reagent, followed by the construction of a complementary DNA (cDNA) library, which was subsequently sequenced on the Illumina NovaSeq 6000 platform (San Diego, CA, USA). Differential expression analysis between the two groups was performed using the DESeq2 R package (version 1.20.0). The resulting *P*-values were adjusted using the Benjamini-Hochberg approach to control the false discovery rate. P adj $\leq$ 0.05 and $|\log2(\text{foldchange})| \geq 1$ were set as the thresholds for significant differential expression.

2.10. Single-cell isolation

Mouse liver tissues were collected, dissected, and enzymatically digested into small pieces using the Liver Dissociation Kit for mouse (130-105-807, MiltenyiBiotec, Germany) for approximately 30 min, following the manufacturer's instructions. The dissociated cells were then passed through a 70 μm strainer and rinsed with 15 mL of Dulbecco's modified Eagle's medium (DMEM/high glucose, VivaCell, Shanghai, China) until a suspension of single cells was obtained. The cells were then collected by centrifugation at 400×*g* for 10 min and resuspended in 1 mL of PBS. The Red Blood Cell Lysis Solution (R1010, Solarbio, China) was used to remove the red blood cells. Afterward, the samples were washed twice with PBS to obtain a single-cell suspension.

2.11. Single-cell RNA sequencing (scRNA-seq)

First, the extracted liver tissues were prepared as single-cell suspensions in accordance with the 10x Genomics® Cell Preparation Guide, after which cell counts and cell viability tests were performed. When cell viability was 80% or higher, the cell concentration was set to 1000 cells/μL. The cell suspensions prepared were collected with microfluidic chips, and droplets encapsulated the beads with cell barcodes and cells. Then, approximately 10,000 cells were captured in droplets to generate nanoliter-scale GEMs (Gel Bead-in-Emulsions). Subsequently, GEMs underwent reverse transcription before cell barcoding, after which the emulsions were disrupted, and the cDNA was isolated and purified further before PCR amplification. The amplified cDNA obtained was subsequently used for library construction. The libraries were further purified, profiled for quality evaluation, and sequenced on the Illumina NovaSeq X plus (San Diego, CA, USA) platform (150 bp paired-end).

2.12. scRNA-seq data pretreatment

Sequencing data were aligned to the mouse reference genome (mm10) using Cell Ranger (version 7.0.0) and then processed with the Seurat R package (version 4.3.0). Due to differences in data quality, low-quality cells were filtered out using sample-specific criteria, and the remaining high-quality cells were selected for further analysis. We embedded high-quality cells within a matrix and clustered them according to similar features. The final step was to visualize and analyze all the clustered cells through the uniform manifold approximation and projection (UMAP) algorithm in scRNA-seq.

2.13. Cell type identification

The expression levels of known canonical markers in each cluster were used to identify different cell types through Seurat's FindAllMarkers function. Clusters containing over 50% of cells with markers for more than one cell type were eliminated, and the remaining cells were re-transformed, re-clustered, and re-annotated.

2.14. Differentially expressed genes (DEGs) and gene functional enrichment analysis

DEG analysis for each cell type was performed using the Seurat FindMarkers function. Using the Seurat VlnPlot function and the R package heatmap, violin plots and heatmaps were generated for further marker visualization. The clusterProfiler R package (version 3.14.0) was utilized to conduct Gene Ontology (GO) and Kyoto Encyclopedia of Genes and Genomes (KEGG) pathway analyses. Significant enrichment was attributed to GO terms or KEGG pathways with a false discovery rate <0.05.

2.15. Flow cytometric analysis

Single-cell suspensions were prepared from Liver and bone marrow, and blocked with purified anti-CD16/CD32 antibody (156,604, BioLegend) for 10 min. The cells were then stained with antibodies recognizing various markers for 30 min at room temperature and analyzed using a CytoFLEX flow cytometer (Beckman Coulter, USA). Anti-CD45 (103,137), anti-CD11b (101,206), anti-F4/80 (123,110), anti-Ly-6G (127,628), anti-Siglec-F (155,508), anti-NK1.1 (108,709), anti-B220 (103,230), anti-CD3 (100,217), anti-CD4 (100,510), anti-CD8 (100,707), and anti-CD146 (134,711) were purchased from BioLegend. Dead cells were excluded by staining with 7-AAD (559,925, BD Pharmingen). We performed analysis using the CytoFLEX flow cytometer (Beckman Coulter) and analyzed the results with CytExpert software. All data are presented as a percentage of total $CD45^+$ cells.

2.16. Preparation of bone marrow-derived macrophages (BMDM)

For preparation of bone marrow-derived macrophages (BMDM), bone marrow was collected from femurs and tibias of mice by flushing with RPMI-1640 media. Bone marrow cells were cultured in RPMI-1640 media with 10% fetal bovine serum (FBS, 10,099-141C, Gibco, USA) and stimulated with 50 ng/mL Macrophage colony-stimulating factor (M-CSF, 315-02, PeproTech) for 7 days to differentiate into BMDM as described previously[28,29].

2.17. Isolation and culture of primary murine liver sinusoidal endothelial cells (LSECs)

Murine LSECs were isolated as described previously[30-32]. In brief, livers of WT mice were perfused with 10 mL of 1 × Hanks' balanced salt solution (HBSS, C0218, Beyotime Biotechnology, Shanghai, China), followed by 0.5 mg/mL DMEM (high glucose)/collagenase type IV (C8160, Solarbio, China) solution, and digested in DMEM (high glucose)/collagenase type IV at 37 °C for 20 min. After filtration through a 70 μm strainer, parenchymal cells were removed by centrifugation at differential speeds. LSECs were isolated using the MojoSort™ Mouse CD146 Selection Kit (480,172, BioLegend). Then, LSECs were seeded onto collagen-coated 24-well plates in DMEM (high glucose) supplemented with 10% FBS, 100 U/mL penicillin, and 0.1 mg/mL streptomycin (SV30010, HyClone, USA) for 24 h to form a monolayer, and subsequently treated with rmPGRN (200 ng/mL) and APAP (5 mmol/L) for 24 h.

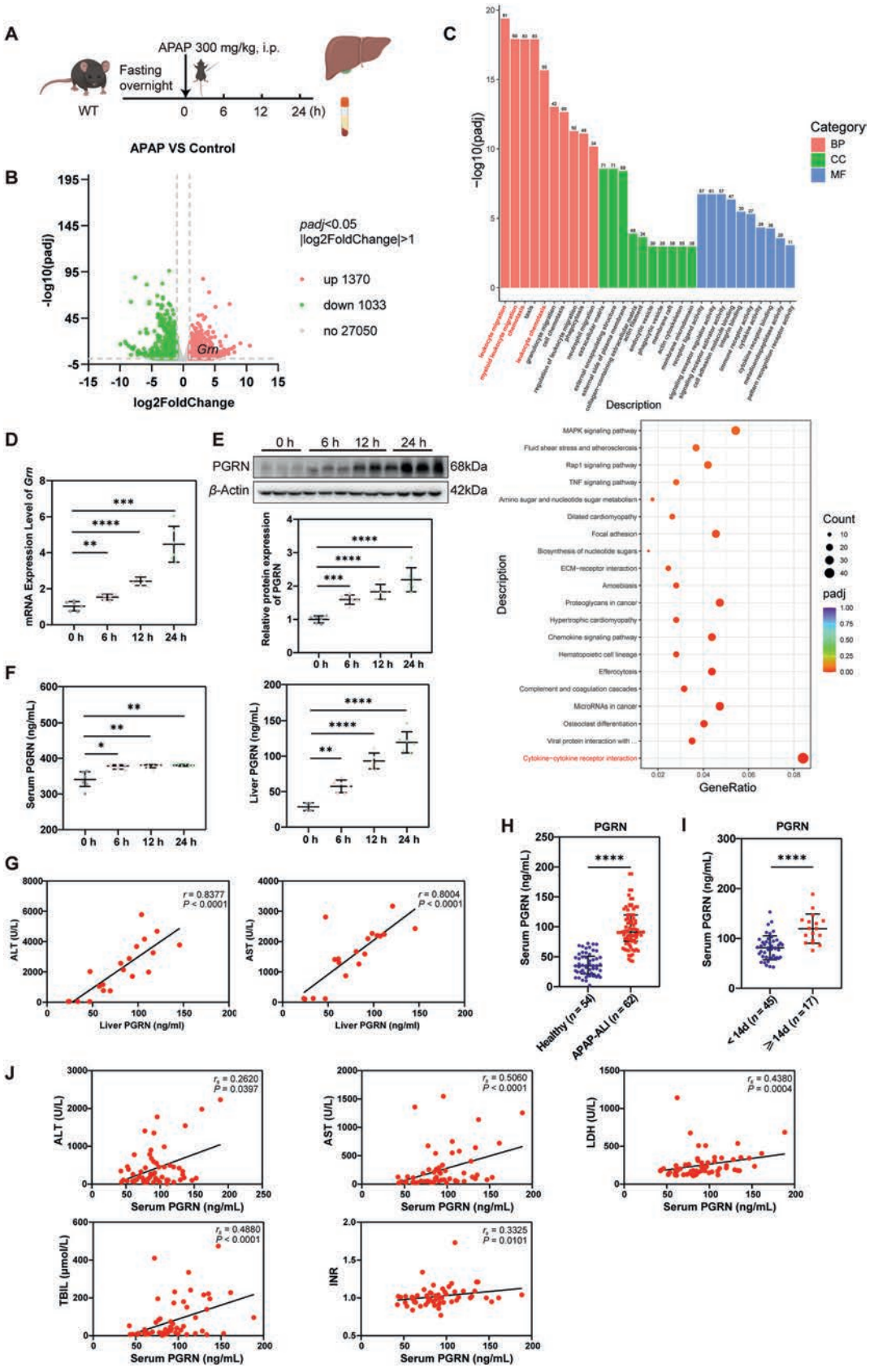

Figure 1 PGRN is increased in mice and human patients in response to acetaminophen (APAP). (A) Schematic diagram of the construction of the APAP-induced acute liver injury (ALI) model. Wild-type (WT) mice were intraperitoneally (i.p.) injected with APAP (300 mg/kg) or phosphate-buffered saline (PBS) as a vehicle control. Liver tissues and serum were collected at 0, 6, 12, and 24 h after APAP treatment. Image

2.18. Isolation of primary mouse hepatocytes (PMHs), nonparenchymal cells (NPCs), and Kupffer cells (KCs)

Primary mouse hepatocytes (NPCs), nonparenchymal cells (NPCs), and Kupffer cells (KCs) were isolated by a two-stage collagenase perfusion method as previously described[33,34]. For PMHs, the hepatic cell suspension was purified by centrifugation using 70% Percoll solution (BS909, Biosharp, China) to acquire viable cells. For NPCs, after filtration through a 70 μm strainer, parenchymal cells were removed by centrifugation at differential speeds. For KCs, the cell suspension was further separated from hepatocytes and other sinusoidal cells by low density gradient centrifugation (50 × *g*, 4 °C) and then cultured with RPMI-1640 media with 10% FBS and 1% penicillin/streptomycin (CM-0212, Procell, Wuhan, China) incubating in a 5% CO_2 atmosphere at 37 °C. Two hours later, the non-adherent cells were washed off gently with PBS, and the remaining adherent cells were KCs.

2.19. Cell culture and treatment

The immortalized human liver sinusoidal endothelial cell (LSEC) line, SK-Hep1, was procured from Procell (CL-0212, Wuhan, China). SK-Hep1 cells were cultured in MEM supplemented with 10% FBS and 1% penicillin/streptomycin (CM-0212, Procell, Wuhan, China) and maintained at 37 °C with 5% CO_2 in an incubator[35]. SK-Hep1 cells were treated with AICAR (200 μmol/L, S1802, Selleck), recombinant human PGRN protein (rhPGRN, 200 ng/mL, 2420-PG, R&D Systems), and APAP (5 mmol/L) for 24 h 293T cells were also procured from the Procell (CL-0005, Wuhan, China), and cultured in DMEM medium containing 10% FBS and 1% penicillin/streptomycin.

The small interfering RNA (siRNA) targeting *Foxo3* was synthesized by GenePharma (GenePharma Co., Ltd., Shanghai, China), and the sequences were as follows: *Foxo3* sense: 5′-AGGGAAGUUUGGUCAAUCATT-3′, antisense: 5′-UGAUUGACCAAACUUCCCUTT-3′. SK-Hep1 cells were transfected with *Foxo3* siRNA or negative control siRNA using the siRNA-Mate plus transfection reagent according to the manufacturer's protocol.

2.20. Quantitative real-time polymerase chain reaction (qRT-PCR)

Total RNA was extracted from liver tissues or cultured cells using TRIzol reagent (TaKaRa Biotechnology). Total RNA was reverse transcribed into cDNA using a reverse transcription kit (HY-K0511A; MedChemExpress). Relative quantitative gene expression was measured with SYBR Green qPCR Master Mix (HY-K0523; MedChemExpress). β-Actin was used as an internal control, and gene expression levels were calculated using the $2^{-\Delta\Delta Ct}$ method. Primers used in this study are listed in Supporting Information Table S4.

2.21. The chromatin immunoprecipitation (ChIP) assay

A ChIP assay was performed using the ChIP Assay kit (26,157, ThermoFisher Scientific, USA) in accordance with the manufacturer's instructions. In brief, mouse livers after APAP intervention were harvested and minced. SK-Hep1 cells were treated with APAP, and the cells were harvested after 24 h. 2×10^7–5×10^7 SK-Hep1 cells were washed twice in cold PBS buffer, livers and cells cross-linked with 1% formaldehyde for 10 min at room temperature, and then quenched by the addition of glycine. Afterwards, samples were lysed, and chromatins were obtained on ice. Chromatin was sonicated to obtain soluble, sheared chromatin (average DNA length of 100–500 bp). 20 μL chromatin was saved at −20 °C for input DNA, and 100 μL of chromatin was used for immunoprecipitation by FOXO3 (66428-1-Ig, Proteintech, Wuhan, China) antibody and IgG antibody (5415, Cell Signaling Technology) to enrich DNA bound to the target protein. 10 μg of antibody was used in the immunoprecipitation reactions at 4 °C overnight. The next day, 30 μL of protein G beads (10004D, Thermo Fisher Scientific, USA) was added, and the samples were further incubated for 3 h. After multiple washes to remove nonspecific proteins and DNA, bound material was then eluted from the beads in 300 μL of elution buffer, treated first with RNase A for 6 h at 65 °C and then with proteinase K (overnight at 45 °C). Immunoprecipitated DNA was amplified by PCR using its specific primers, and the enriched DNA fragments were then analyzed by qPCR to assess the strength of protein-DNA interactions. All primers are listed in Table S4.

2.22. Dual luciferase reporter assay

The dual luciferase assay was conducted following standard procedures (Promega, Madison, USA). The day before transfection, 293T cells were seeded in 24-well plates to ensure that the cell density at the time of transfection was 60%–70%. The *Il33* full-length, *Il33*-WT, and *Il33*-MT constructs were cloned into the pGL3-basic vector containing Firefly luciferase; the *Foxo3*-CDS

created with BioRender.com. (B) Volcano plot of differential analysis of high-throughput sequencing data. Red dots represent up-regulated genes, green dots represent down-regulated genes, and gray dots represent genes with no significant differential expression ($n = 5$ independent biological replicates per group). (C) Gene Ontology (GO) including biological process (BP), cellular component (CC), and molecular function (MF), and Kyoto Encyclopedia of Genes and Genomes (KEGG) enrichment analysis of upregulated differentially expressed genes. (D) Relative mRNA levels of *Grn* expression in the liver of WT mice at 0, 6, 12, and 24 h after APAP treatment ($n = 6$ independent biological replicates per group). (E) Western blot and densitometry analysis of PGRN in the liver of WT mice at 0, 6, 12, and 24 h after APAP treatment ($n = 6$ independent biological replicates per group). (F) The protein levels of PGRN in serum and liver tissues were quantified by enzyme-linked immunosorbent assay (ELISA) at 0, 6, 12, and 24 h after APAP treatment ($n = 4$–6 independent biological replicates per group). (G) Correlation between PGRN concentration in liver and serum alanine aminotransferase (ALT) and aspartate aminotransferase (AST) concentrations in APAP-induced ALI mice. (H) Admission concentrations of PGRN were measured by ELISA in serum samples collected from 62 patients with APAP overdose and 54 healthy controls. (I) Admission concentrations of PGRN in serum samples collected from patients with a hospital stay <14 days and those with a hospital stay ≥14 days. (J) Correlation of admission PGRN concentrations with ALT, AST, lactate dehydrogenase (LDH), total bilirubin (TBIL), and international normalized ratio (INR) values in the patients with APAP-ALI. Except for clinical research (H–J), data are representative of triplicate independent experiments. Data are presented as mean ± SD or median with interquartile range (IQR). $^*P < 0.05$, $^{**}P < 0.01$, $^{***}P < 0.001$, $^{****}P < 0.0001$ *versus* the indicated groups. *P* values were calculated based on the Kruskal–Wallis test, one-way ANOVA, nonparametric Mann–Whitney U test, Pearson correlation coefficient (*r*), or Spearman correlation coefficient (r_s).

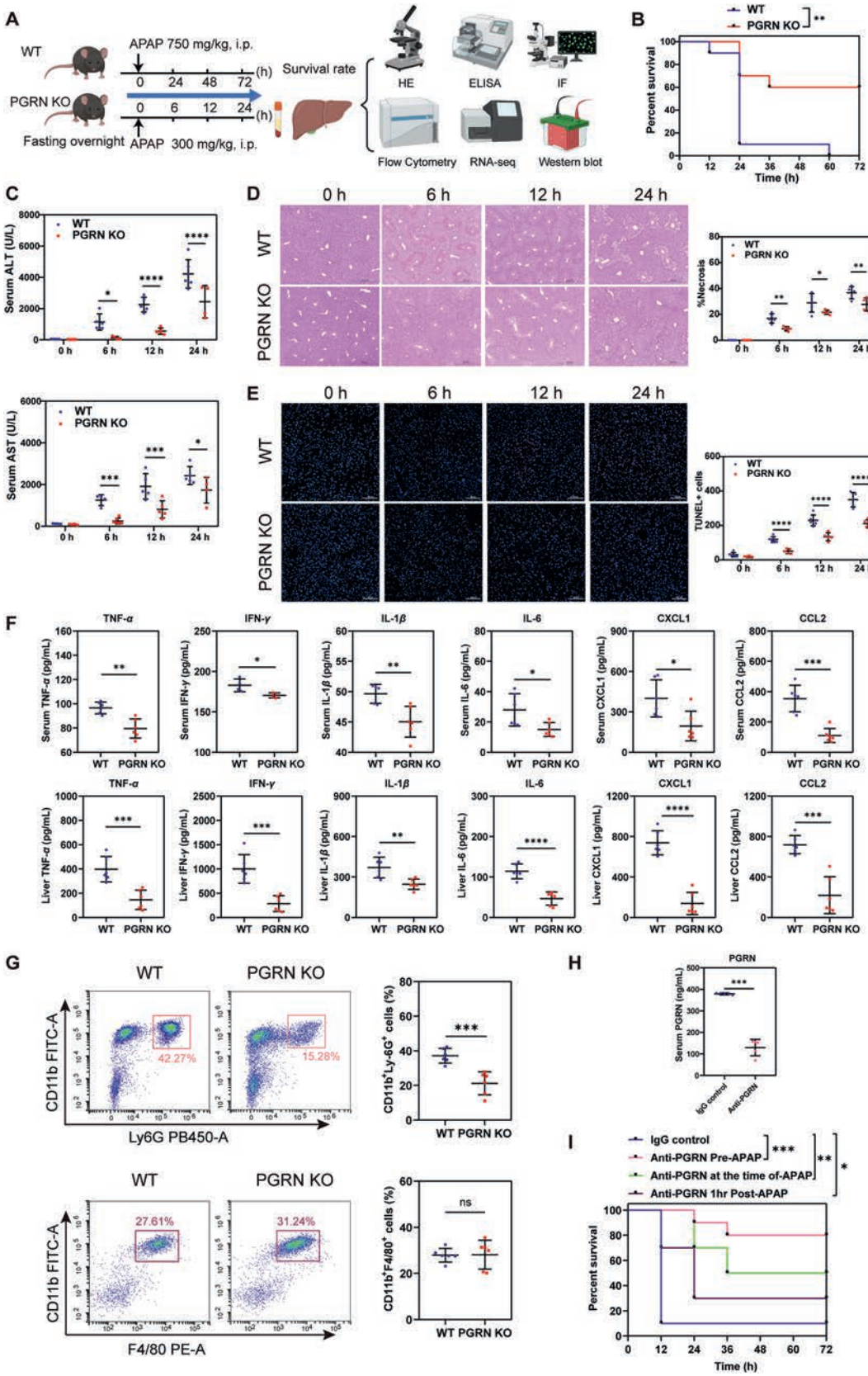

Figure 2 PGRN loss protects from liver injury induced by APAP. (A) Schematic diagram of the construction of APAP-induced ALI model in PGRN KO mice and WT littermates. Image created with BioRender.com. (B) Survival of PGRN KO mice and WT littermates at 0, 12, 24, 36, 48, 60, and 72 h after APAP treatment (APAP = 750 mg/kg, n = 15 independent biological replicates per group). (C) Serum concentrations of ALT and AST in PGRN KO mice and WT littermates were measured at 0, 6, 12, and 24 h after APAP treatment (n = 4−6 independent biological

region sequence gene was cloned into the pcDNA3.1 vector; and the pRL-TK plasmid contained Renilla luciferase. All the plasmids were transfected into 293T cells (gene sequences are listed in Supporting Information Table S5). After 48 h, the cells were lysed, and the firefly luciferase activity was measured using the Dual-Luciferase® Reporter Assay System (Promega) and normalized to Renilla luciferase as the internal reference.

2.23. Phosphorylation site mutation of FOXO3

The mutant protein of FOXO3 (S413A) was constructed using a commercial point mutagenesis kit (D0206M, Beyotime Biotechnology, Shanghai, China) with seamless cloning and mutagenic primers. S413A: By a codon point mutation, the serine residue (S) at position 413 of FOXO3 is turned into an alanine residue (A), which cannot be phosphorylated, thus mimicking FOXO3 with no phosphorylation at S413. The FOXO3-WT and FOXO3-S413A were conjugated with a His tag. All the plasmids were transfected into SK-Hep1 cells with Lipo8000™ (C0533, Beyotime Biotechnology, Shanghai, China) according to the manufacturer's instructions (gene sequences are listed in Supporting Information Table S6). Twenty-four hours later, the cells were treated with AICAR (200 μmol/L), rhPGRN (200 ng/mL), and APAP (5 mmol/L) for 24 h.

2.24. Western blot assay

Liver tissues and cell samples were homogenized in RIPA lysis buffer (P0013B, Beyotime Biotechnology, Shanghai, China) containing protease and phosphatase inhibitors (P1045, Beyotime Biotechnology, Shanghai, China) for 30 min on ice. After centrifugation at 12,000×g for 15 min at 4 °C, the supernatant was collected, and the protein concentrations were quantified with a BCA protein assay kit (P0010, Beyotime Biotechnology, Shanghai, China). Proteins from each sample were loaded and separated by SDS-PAGE gels and transferred to polyvinylidene fluoride (PVDF) membranes (Millipore, Billerica, MA, USA). After blocking, membranes were incubated overnight at 4 °C with primary antibodies against PGRN (AF2557, R&D Systems), CYP2E1 (19937-1-AP, Proteintech), AMPK (5831, Cell Signaling Technology), p-AMPK (2535, Cell Signaling Technology), FOXO3 (2497, Cell Signaling Technology), p-FOXO3 (8174, Cell Signaling Technology), IL-33 (YT5487, Immunoway, USA), Lamin B1 (66095-1-Ig, Proteintech), 6X His tag (HA722798, HuaAn Biotechnology), and β-actin (66009-1-Ig, Proteintech). The next day, the membranes were washed and incubated with goat anti-mouse IgG (H + L) secondary antibody (C31430100, ThermoFisher Scientific, USA), goat anti-rabbit IgG (H + L) secondary antibody (C31460100, Thermo Fisher Scientific, USA), and donkey anti-sheep IgG (H + L) secondary antibody (713-035-147, Jackson ImmunoResearch) at room temperature for 1 h. Proteins were visualized using enhanced chemiluminescence (ECL, ZENBIO Biotechnology, China). The relative intensities of the protein bands were analyzed using the Bio-Rad Quantity One software. The results were normalized to β-actin or Lamin B1 levels.

2.25. Statistics analysis

All data are presented as mean ± standard deviation (SD) or median with interquartile range (IQR). The sample size (n) for each experiment represents biological replicates, as indicated in the figure legends. The chi-square test was used for the assessment of qualitative variables. All quantitative variables were tested for normality with the Shapiro−Wilk normality test. For the homogeneity of variance test, the F test was used for two groups, and the Brown−Forsythe test was used for multiple groups. The student's t-test was applied to compare two normally distributed groups, and the Mann−Whitney U test was applied to compare two groups that did not conform to normal distribution. For comparisons among multiple groups, one-way or two-way ANOVA with appropriate *post hoc* tests was applied to data that met the normal distribution. For data that did not follow a normal distribution, the Kruskal−Wallis test with Dunn's *post hoc* test was used. For survival analysis, Kaplan−Meier analysis was performed, followed by the log-rank test. Pearson correlation coefficient (r) and Spearman correlation coefficient (r_s) were used to evaluate the correlations. Statistical analyses were performed with SPSS 26.0 and GraphPad Prism 8.0 software. In all analyses, statistical significance was set at $P < 0.05$, and all tests were two-tailed. Details of statistical tests are included in the figure legends.

3. Results

3.1. PGRN is increased in mice and human patients in response to APAP

To study host-derived gene expression changes in a murine model of APAP-induced ALI, we performed RNA-sequencing analysis in the livers of mice (Fig. 1A). The volcano plot from the sequencing results showed that a total of 1370 genes were up-regulated and 1033 genes were down-regulated, and PGRN was one of the up-regulated genes after APAP overdose (Fig. 1B). Further Gene Ontology (GO) and Kyoto Encyclopedia of Genes and Genomes (KEGG) enrichment analysis revealed that the biological processes (BP) of APAP-induced ALI mice were mainly concentrated in immune processes (Fig. 1C). Quantitative PCR, Western blot

replicates per group). (D) Liver necrosis was evaluated and quantified at 0, 6, 12, and 24 h after APAP treatment (n = 4−6 independent biological replicates per group; scale bar, 500 μm). (E) APAP-induced hepatocyte apoptosis in PGRN KO mice and WT littermates was detected by terminal deoxynucleotidyl transferase-mediated dUTP nick end labeling (TUNEL) assay at 0, 6, 12, and 24 h after APAP treatment (n = 4−6 independent biological replicates per group; scale bar, 500 μm). (F) Protein expression levels of TNF-α, IFN-γ, IL-1β, IL-6, CXCL1, and CCL2 in serum and liver tissues at 24 h after APAP treatment were measured by ELISA (n = 4−6 independent biological replicates per group). (G) Flow cytometric analysis images and the corresponding quantification of the percentages of neutrophils ($CD11b^+Ly6G^+$) and macrophages ($CD11b^+F4/80^+$) in hepatic $CD45^+$ cells at 24 h after APAP treatment (n = 6 independent biological replicates per group). (H) WT mice were injected intraperitoneally (i.p.) with anti-mouse PGRN antibody, and the expression level of PGRN in serum was measured by ELISA (n = 5 independent biological replicates per group). (I) Survival of WT mice treated with or without anti-PGRN antibody at 0, 12, 24, 36, 48, 60, and 72 h after APAP treatment (APAP = 600 mg/kg, n = 15 independent biological replicates per group). All data are representative of triplicate independent experiments. Data are presented as mean ± SD. *$P < 0.05$, **$P < 0.01$, ***$P < 0.001$, ****$P < 0.0001$, ns, not significant *versus* the indicated groups. P values were calculated based on log-rank test, two-way ANOVA, or two-tailed unpaired Student's t-test.

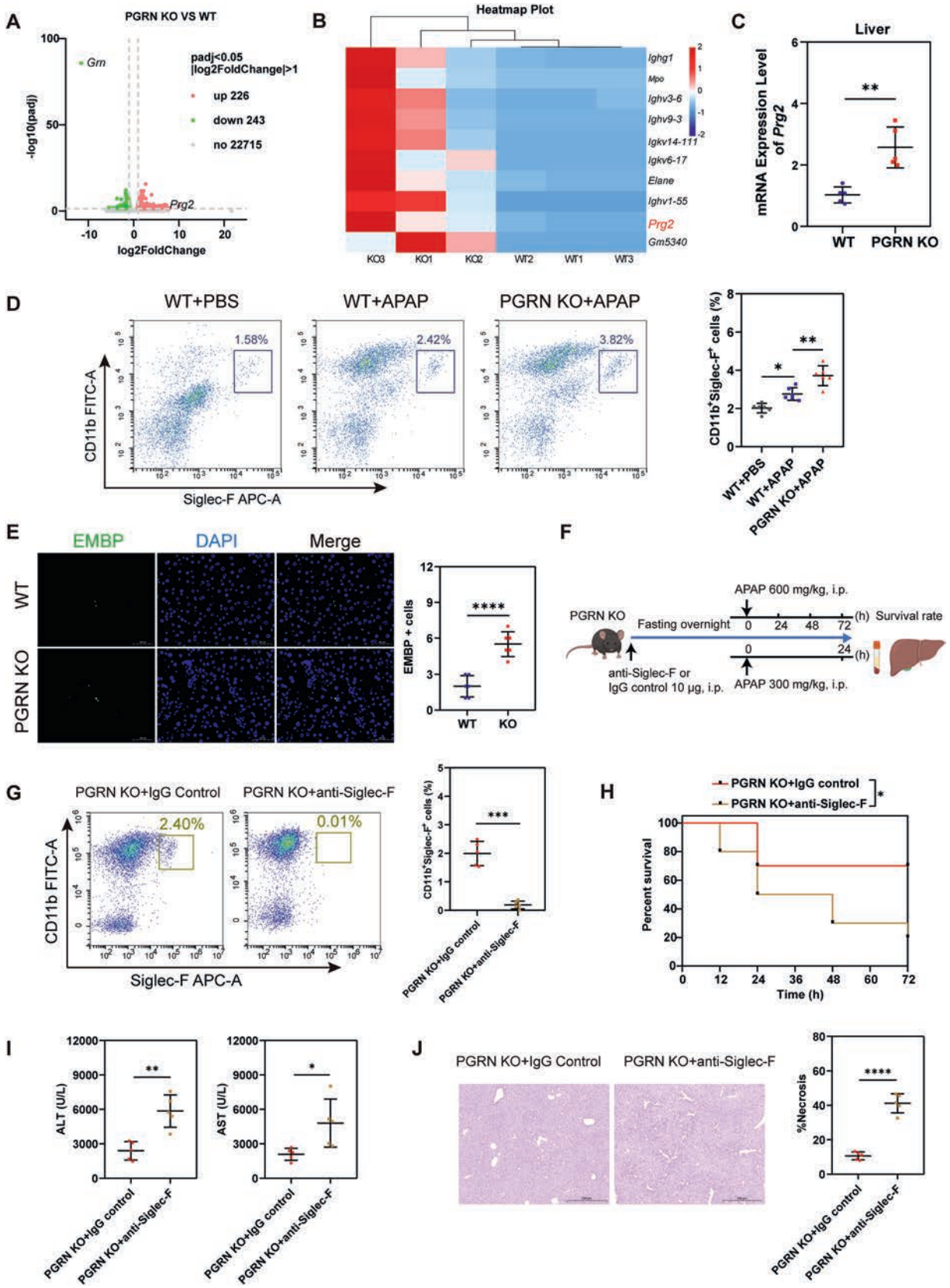

Figure 3 PGRN loss improves APAP-induced ALI in an eosinophil-dependent manner. (A) Volcano plot of differential analysis of high-throughput sequencing data. Red dots represent up-regulated genes, green dots represent down-regulated genes, and gray dots represent genes with no significant differential expression ($n = 3$ independent biological replicates per group). (B) Heatmap of differential analysis of high-throughput sequencing data showed the top 10 upregulated genes in the livers of PGRN KO mice compared with WT littermates. (C)

and ELISA confirmed up-regulation of hepatic PGRN in response to APAP (Fig. 1D−F), and serum protein levels PGRN were also increased by APAP (Fig. 1F). Interestingly, liver PGRN concentrations were positively correlated with ALT and AST levels, biomarkers of liver damage (Fig. 1G). To further confirm the elevation of PGRN in the animals after APAP overdose, we examined PGRN levels in a cohort of 62 patients with APAP overdose (Table S1). At the time of hospital admission, serum PGRN levels were significantly higher than those in healthy controls (Fig. 1H). Moreover, admission serum PGRN concentrations of patients whose hospital stay was $\geq$14 days were significantly higher than those in patients whose hospital stay was $<$14 days (Fig. 1I). There was a significant correlation of serum PGRN levels with ALT, AST, lactate dehydrogenase (LDH), total bilirubin (TBIL), or international normalized ratio (INR) values in APAP overdose patients (Fig. 1J). To confirm the up-regulation of PGRN in a larger patient cohort, we obtained DILI patient serum samples from another cohort consisting of 103 patients (Table S2). Admission serum concentrations of PGRN were significantly increased compared with those in healthy controls (Supporting Information Fig. S1A), especially in DILI patients with hospital stay $\geq$14 days (Fig. S1B), which significantly correlated with ALT, AST, LDH, TBIL, or INR in DILI patients (Fig. S1C). Together, these findings indicate that PGRN is induced in both a mouse model and human patients with APAP overdose, which may serve as a new biomarker related to liver injury.

3.2. *PGRN loss protects from liver injury induced by APAP*

The functional role of PGRN was examined in an animal model of APAP-induced ALI using mice with germline knockout (KO) of PGRN and their WT littermates as controls (Fig. 2A). We studied a similar number of both male and female mice. Genotyping and Western blot analysis showed that PGRN was markedly knocked out at both genomic and translational levels (Supporting Information Fig. S2A and S2B). Circulating PGRN protein levels were also dramatically decreased in PGRN KO mice (Fig. S2C). The survival rate of PGRN KO mice was dramatically higher than WT littermates upon challenge with a 750 mg/kg dose of APAP (Fig. 2B). Compared with WT littermates, PGRN KO mice developed much less severe liver injury, evident by a decreased elevation of serum ALT and AST levels (Fig. 2C), as well as less expansive areas of necrosis after APAP treatment (Fig. 2D). Consistently, TUNEL also demonstrated fewer hepatic cell apoptosis in PGRN KO mice (Fig. 2E). Similarly, female KO mice also had lower mortality, ALT and AST levels, as well as smaller necrotic areas (Supporting Information Fig. S3). An acute inflammatory response is a detrimental hallmark of APAP-induced ALI[36]. We also found that PGRN loss resulted in an attenuation of local and systemic inflammation, evident by a reduced elevation of serum and hepatic production of cytokines and chemokines, including TNF-α, IFN-γ, IL-1β, IL-6, CXCL1, and CCL2 (Fig. 2F), as well as a significantly decreased number of hepatic $CD11b^+Ly6G^+$ neutrophils after APAP administration (Fig. 2G and Supporting Information Fig. S4). However, PGRN KO and WT mice displayed comparable hepatic $CD11b^+F4/80^+$ macrophages (Fig. 2G), hepatic lymphocytes, including $CD4^+$/$CD8^+$ T cells, B cells, and natural killer (NK) T cells (Supporting Information Fig. S5). Hepatic GSH, CYP2E1 protein levels, and CYP2E1 activity were comparable after APAP treatment in both genotypes (Supporting Information Fig. S6A−S6D), suggesting that PGRN did not affect the metabolic conversion of APAP. Together, these results demonstrated that PGRN loss ameliorates liver injury by reducing the inflammatory responses rather than by affecting APAP metabolism. As an alternative approach to genetic deletion of PGRN, we treated WT mice with an anti-PGRN antibody before APAP challenge, which could significantly reduce serum PGRN levels after APAP treatment (Fig. 2H). Compared with IgG-treated controls, mice treated with anti-PGRN had a significantly lower mortality rate after APAP treatment (Fig. 2I). Interestingly, anti-PGRN administration at the time of or 1 h after APAP-induced ALI significantly improved survival, suggesting that anti-PGRN administration is a viable therapeutic modality in APAP-induced ALI as a means of improving survival. Collectively, these findings indicate that PGRN deficiency plays a protective role in APAP-induced ALI. In addition, the protection of PGRN loss in hepatoprotection was also observed in another model of ConA-induced hepatic injury, based on survival, pathological evaluations, and ALT/AST levels in PGRN KO mice or WT mice treated with anti-PGRN antibody (Supporting Information Fig. S7).

3.3. *Supplementation of recombinant PGRN protein aggravates APAP-induced ALI*

To validate observations in PGRN KO mice and confirm PGRN loss as the basis for the protection in PGRN KO mice, we supplemented WT mice with rmPGRN upon APAP challenge (Supporting Information Fig. S8A), which could significantly increase circulating PGRN levels (Fig. S8B). The survival rate of rmPGRN-treated mice was significantly lower than vehicle-treated mice upon challenge with a 500 mg/kg dose of APAP (Fig. S8C). Mice treated with rmPGRN after APAP overdose had worse livers than APAP control mice, as indicated by significantly increased ALT and AST induction (Fig. S8D), and hepatic necrosis

Relative mRNA levels of *Prg2* in the liver of PGRN KO mice and WT littermates at 24 h after APAP treatment ($n = 5$ independent biological replicates per group). (D) Flow cytometric analysis images and the corresponding quantification of the percentages of eosinophils ($CD11b^+$Siglec-F^+) in hepatic $CD45^+$ cells at 24 h after APAP treatment ($n = 6$ independent biological replicates per group). (E) Immunofluorescence staining of EMBP (green) and DAPI (blue) in liver tissue and the quantification of the percentage of $EMBP^+$ cells at 24 h after APAP treatment ($n = 6$ independent biological replicates per group; scale bar, 50 μm). (F) Schematic diagram of anti-mouse Siglec-F antibody administration in PGRN KO mice. Image created with BioRender.com. (G) Flow cytometric analysis images and the corresponding quantification of the percentages of eosinophils ($CD11b^+$Siglec-F^+) in hepatic $CD45^+$ cells at 24 h after APAP treatment ($n = 5$ independent biological replicates per group). (H) Survival rate of mice at 0, 12, 24, 36, 48, 60, and 72 h after APAP treatment (APAP = 600 mg/kg, $n = 15$ independent biological replicates per group). (I) Serum ALT and AST levels in PGRN KO mice treated with or without anti-Siglec-F antibody at 24 h after APAP treatment ($n = 5$ independent biological replicates per group). (J) Liver necrosis was evaluated and quantified at 24 h after APAP treatment ($n = 5$ independent biological replicates per group; scale bar, 500 μm). All data are representative of triplicate independent experiments. Data are presented as mean ± SD. $^*P < 0.05$, $^{**}P < 0.01$, $^{***}P < 0.001$, $^{****}P < 0.0001$ *versus* the indicated groups. *P* values were calculated based on log-rank test, one-way ANOVA, or two-tailed unpaired Student's *t*-test.

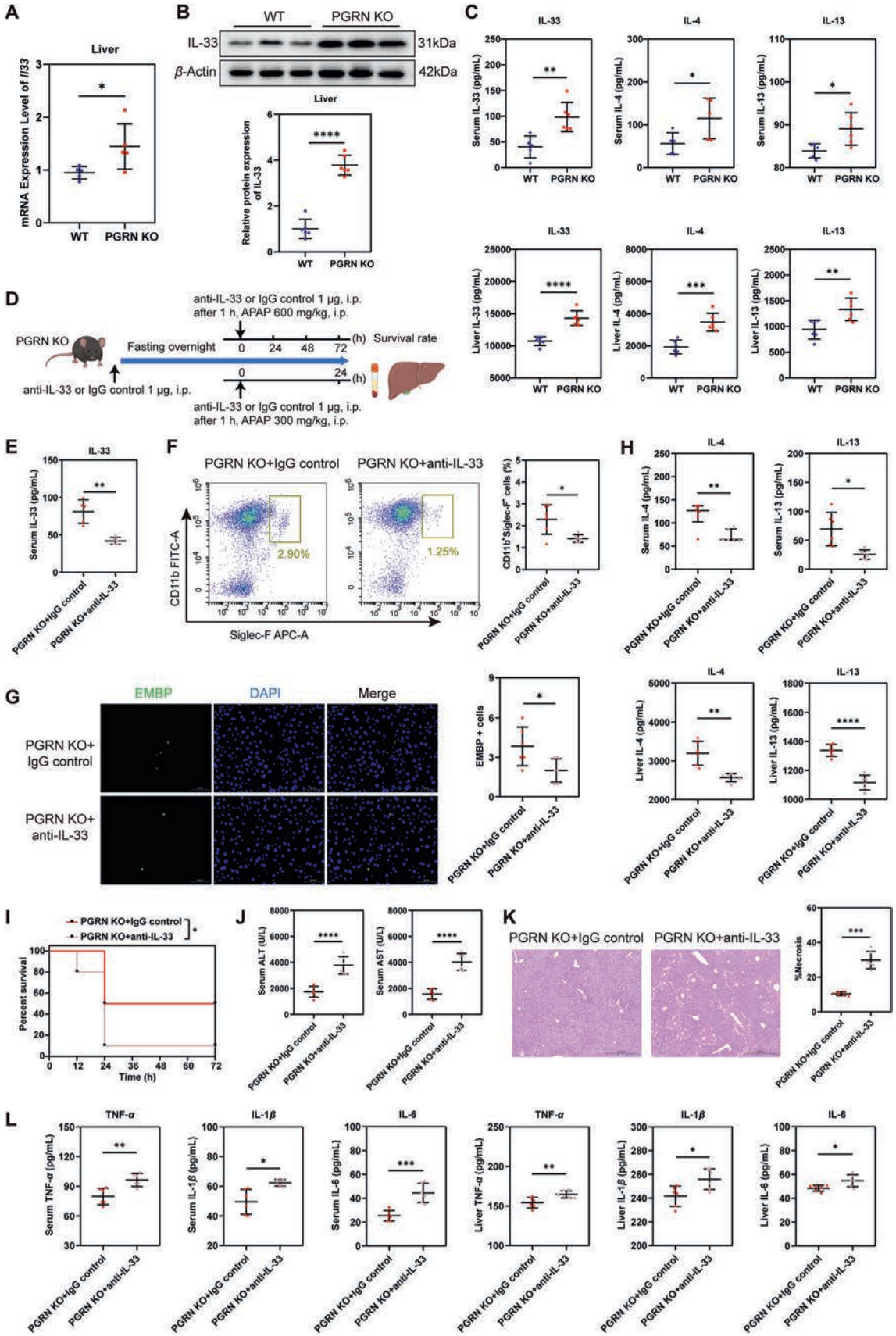

Figure 4 PGRN loss attenuates APAP-induced ALI through IL-33-dependent eosinophil recruitment. (A) Relative mRNA levels of *Il33* in the liver of PGRN KO mice and WT littermates at 24 h after APAP treatment ($n = 5$ independent biological replicates per group). (B) Western blot

(Fig. S8E), as well as cell apoptosis in the liver (Fig. S8F). Besides, rmPGRN treatment increased hepatic and serum concentrations of TNF-α, IL-1β, and IL-6 (Fig. S8G), and augmented hepatic infiltration of $CD11b^+Ly6G^+$ neutrophils after APAP administration (Fig. S8H). But there was no significant effect on the number of hepatic $CD11b^+F4/80^+$ macrophages (Fig. S8H). To further explore whether PGRN mediates its harmful effects through the recruitment of neutrophils and macrophages, we depleted neutrophils and macrophages in rmPGRN-treated mice. The results showed that depletion of neutrophils and macrophages did not attenuate rmPGRN-induced APAP-ALI, suggesting that rmPGRN does not mediate its harmful effects through neutrophils and macrophages (Supporting Information Fig. S9).

3.4. PGRN loss improves APAP-induced ALI in an eosinophil-dependent manner

To characterize the molecular mechanisms accounting for the protective function of PGRN loss, we compared gene expression profiles between livers from PGRN KO mice and WT littermates after APAP overdose. The volcano plot showed that a total of 226 genes were up-regulated and 243 genes were down-regulated in the livers of PGRN KO mice compared with WT littermates (Fig. 3A). The gene *Prg2*[37], encoding eosinophil major basic protein (MBP), was one of the top 10 up-regulated genes (Fig. 3B), as confirmed by quantitative PCR analyses (Fig. 3C). We then focused on hepatic eosinophils, and observed that the number of eosinophils ($CD11b^+Siglec\text{-}F^+$ cells) in the liver was significantly increased in PGRN KO mice compared with WT littermates (Fig. 3D and Fig. S4), and the number of cells expressing EMBP was also higher in PGRN KO mice than that in WT littermates after APAP challenge (Fig. 3E). Besides, the increase of hepatic eosinophils ($CD11b^+Siglec\text{-}F^+$ cells) was also observed in PGRN KO mice compared with WT littermates in ConA-induced hepatic injury (Supporting Information Fig. S10).

To investigate the functional role of eosinophils in the protection against APAP-induced ALI mediated by PGRN loss, we depleted these cells by an intraperitoneal injection of an anti-Siglec-F antibody as previously reported[38], whereas control mice were treated with an irrelevant IgG control (Fig. 3F). As shown in Fig. 3G, eosinophils were effectively depleted from the liver before APAP challenge. We found that depletion of eosinophils could significantly increase the mortality rate of PGRN KO mice after APAP treatment (Fig. 3H). Eosinophil-depleted PGRN KO mice exhibited much more severe APAP-induced ALI compared with non-depleted mice, as demonstrated by marked increases in serum ALT and AST levels (Fig. 3I), as well as tissue necrosis (Fig. 3J). Together, these data revealed a crucial role for eosinophils in mediating liver protection elicited by PGRN loss during APAP overdose.

3.5. PGRN loss attenuates APAP-induced ALI through IL-33-dependent increase of eosinophil recruitment

To understand the mechanism by which PGRN loss enhanced eosinophil recruitment, we hypothesized that IL-33 might play an important role in recruiting eosinophils in PGRN KO mice. IL-33 has been identified as an essential mediator in inducing eosinophil recruitment after ALI[39]. As expected, the mRNA and protein expression of IL-33 were significantly elevated in the liver of PGRN KO mice compared with WT littermates after APAP challenge (Fig. 4A and B). Moreover, the increased production of IL-33 in PGRN KO mice was further confirmed by detecting the up-regulated levels of hepatic and serum IL-33 by ELISA (Fig. 4C). It has been shown that eosinophils represent a major cellular source of IL-4 and IL-13, which played a critical role in mediating hepatoprotection of eosinophils[40], we also found that PGRN KO mice produced significantly higher levels of IL-4 and IL-13 after APAP overdose (Fig. 4C). These findings led to our hypothesis that the increase of IL-33 production contributes to enhanced hepatic eosinophil infiltration in PGRN KO mice. To examine this hypothesis, we treated PGRN KO mice with anti-IL-33 neutralizing antibody before APAP challenge (Fig. 4D), and found that a significant decrease in serum IL-33 levels compared with IgG-treated control mice (Fig. 4E). Anti-IL-33-treated PGRN KO mice displayed significantly reduced eosinophil recruitment into the liver (Fig. 4F and G), which was accompanied with lower levels of IL-4 and IL-13 (Fig. 4H). More importantly, survival assays in the APAP-induced ALI mouse model showed significantly decreased survival in PGRN KO mice treated with anti-IL-33 antibody (Fig. 4I). Consistently, anti-IL-33-treated PGRN KO mice developed worsened liver injury, as demonstrated by increased serum levels of ALT and AST (Fig. 4J), as well as areas of hepatocyte necrosis (Fig. 4K). In contrast to reduced IL-4 and IL-13 levels, anti-IL-33 treatment increased production of TNF-α, IL-1β, and IL-6 in PGRN KO mice after APAP challenge (Fig. 4L).

and densitometry analysis of IL-33 in the liver of PGRN KO mice and WT littermates at 24 h after APAP treatment ($n = 6$ independent biological replicates per group). (C) The levels of IL-33, IL-4, and IL-13 in serum and liver tissues at 24 h after APAP treatment were determined by ELISA ($n = 5-6$ independent biological replicates per group). (D) Schematic diagram of anti-mouse IL-33 antibody administration in PGRN KO mice. Image created with BioRender.com. (E) The expression level of IL-33 in serum at 24 h after APAP treatment was detected by ELISA, treated with or without anti-IL-33 antibody ($n = 5$ independent biological replicates per group). (F) Flow cytometric analysis and the corresponding quantification of the percentages of eosinophils ($CD11b^+Siglec\text{-}F^+$) in hepatic $CD45^+$ cells at 24 h after APAP treatment ($n = 6$ independent biological replicates per group). (G) Immunofluorescence staining of EMBP (green) and DAPI (blue) in liver tissues and quantification analysis of the percentage of $EMBP^+$ cells at 24 h after APAP treatment ($n = 6$ independent biological replicates per group; scale bar, 50 μm). (H) The levels of IL-4 and IL-13 in serum and liver tissues at 24 h after APAP treatment were determined by ELISA ($n = 6$ independent biological replicates per group). (I) Survival rate of mice at 0, 12, 24, 36, 48, 60, and 72 h after APAP treatment (APAP = 600 mg/kg, $n = 15$ independent biological replicates per group). (J) Serum ALT and AST levels in PGRN KO mice treated with or without anti-IL-33 antibody at 24 h after APAP treatment ($n = 6$ independent biological replicates per group). (K) Liver necrosis was evaluated and quantified at 24 h after APAP treatment ($n = 6$ independent biological replicates per group; scale bar, 500 μm). (L) Expression levels of inflammatory factors TNF-α, IL-1β, and IL-6 in serum and liver tissues at 24 h after APAP treatment were measured by ELISA ($n = 6$ independent biological replicates per group). All data are representative of triplicate independent experiments. Data are presented as mean ± SD. $^*P < 0.05$, $^{**}P < 0.01$, $^{***}P < 0.001$, $^{****}P < 0.0001$ *versus* the indicated groups. *P* values were calculated based on the log-rank test or two-tailed unpaired Student's *t*-test.

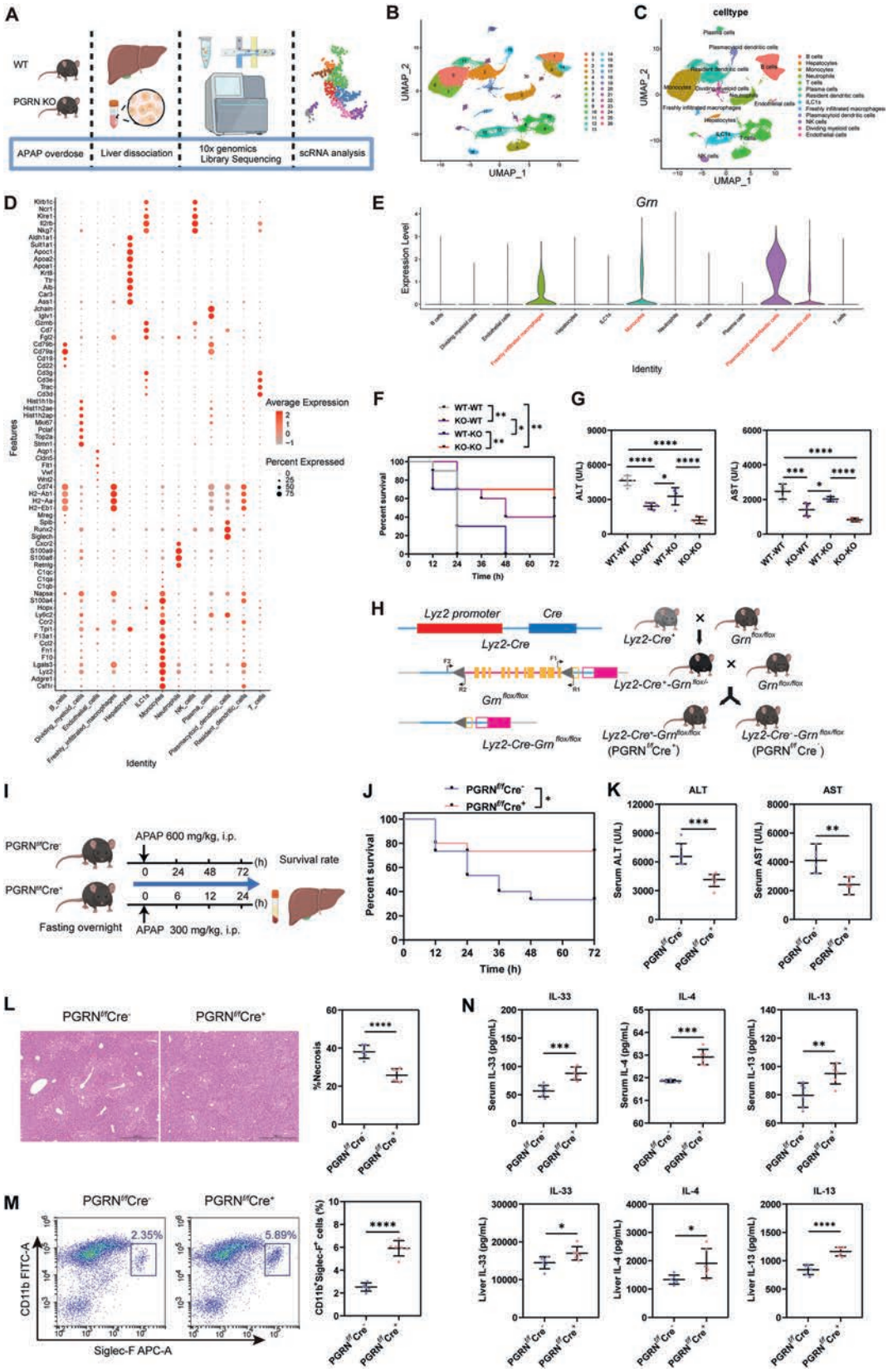

Figure 5 Myeloid-specific deletion of PGRN protects against APAP-induced ALI. (A) The study protocol is shown. Livers obtained from PGRN KO mice and WT littermates at 24 h after APAP treatment ($n = 3$ independent biological replicates per group) were analyzed by scRNA-seq. Image created with BioRender.com. (B, C) The clustering of cells by uniform manifold approximation and projection (UMAP) is shown after unsupervised clustering with a Graphcluster algorithm. (D) Dot plot of the mean expression of canonical marker genes for the 13 major lineages as indicated. (E) Violin plots show *Grn* levels in each cell type. (F) Bone-marrow cells from PGRN KO and WT mice were intravenously injected

3.6. PGRN aggravates APAP-induced ALI by suppressing eosinophil recruitment through the inhibition of IL-33

In WT mice after APAP challenge, we observed similar decreased recruitment of eosinophils to the liver by rmPGRN (Supporting Information Fig. S11A and S11B), which was related to reduced expression of IL-33, IL-4, and IL-13 (Fig. S11C and S11D). We then treated WT mice *in vivo* with rmPGRN or the combination of rmPGRN and rmIL-33 (Fig. S11E), and injecting exogenous rmIL-33 could restore IL-33 levels in rmPGRN-treated mice (Fig. S11F). For WT mice in the presence of rmPGRN, rmIL-33 decreased mortality after APAP overdose (Fig. S11G). The observation is consistent with the liver injury after APAP overdose being attenuated in rmPGRN-treated mice (Fig. S11H and S11I). Hepatic and circulating TNF-α, IL-1β, and IL-6 levels in rmPGRN-treated mice were also decreased by rmIL-33 treatment (Fig. S11J). Furthermore, rmIL-33 administration enhanced hepatic eosinophil infiltration of rmPGRN-treated mice after APAP overdose (Fig. S11K and S11L), which was associated with increased levels of IL-4 and IL-13 (Fig. S11M). These data, together with those from anti-IL-33 treatment in PGRN KO mice, suggest that the PGRN−IL-33 axis is critically involved in the hepatoprotective function of eosinophils.

3.7. Myeloid-specific deletion of PGRN protects against APAP-induced ALI

To identify the main cellular source involved in the PGRN−IL-33 axis, we performed scRNA-seq using liver tissues isolated from PGRN KO mice and WT littermates (Fig. 5A). After quality control and standard data processing, downstream analysis was conducted on 51,759 cells, including 26,537 cells in WT mice and 25,222 cells in PGRN KO mice. The uniform manifold approximation and projection (UMAP) plot showed that liver samples of the PGRN KO and WT mice were mainly divided into 26 cell clusters (Supporting Information Fig. S12A), while the heatmap showed the top 5 marker genes in each cell cluster (Fig. S12B). Next, each cell cluster was annotated with marker genes, resulting in the identification of 13 cell types from these 26 clusters, which mainly included B cells, hepatocytes, monocytes, neutrophils, T cells, plasma cells, resident dendritic cells, type 1 innate lymphoid cells (ILC1s), freshly infiltrated macrophages, plasmacytoid dendritic cells, NK cells, dividing myeloid cells, and endothelial cells (Fig. 5B and C). The dot plot showed the typical marker genes of each cell type (Fig. 5D), while the volcano plot illustrated the differentially expressed genes in the main cell types of PGRN KO mice compared with WT littermates (Fig. S12C). We then analyzed the expression of PGRN in 13 cell types, showing that PGRN expression was detected primarily in myeloid subsets, including macrophages, monocytes, plasmacytoid dendritic cells, and resident dendritic cells (Fig. 5E).

To determine if the expression of PGRN in myeloid cells plays an important role in APAP-induced ALI, we generated BM-chimeric mice by reconstituting lethally irradiated WT mice with syngeneic PGRN KO BM or PGRN KO mice with WT BM. Transplantation of PGRN KO BM into irradiated WT or PGRN KO recipients significantly enhanced the survival of APAP-induced ALI relative to mice receiving WT BM (Fig. 5F). Additionally, irradiated WT and PGRN KO mice reconstituted with PGRN KO BM displayed a significant reduction in the levels of ALT and AST relative to mice receiving WT BM (Fig. 5G). These data therefore suggest that PGRN derived from the hematopoietic cell compartment contributed to increase APAP-induced ALI. Next, we generated myeloid-specific PGRN conditional KO mice ($PGRN^{f/f}Cre^{+}$ mice) to delete PGRN in myeloid cells. Their littermates ($PGRN^{f/f}Cre^{-}$mice) served as controls (Fig. 5H). Loss of PGRN in bone marrow-derived macrophages from $PGRN^{f/f}Cre^{+}$ mice was verified (Supporting Information Fig. S13A and S13B), and circulating PGRN levels were also dramatically decreased in $PGRN^{f/f}Cre^{+}$ mice (Fig. S13 C). Myeloid-specific PGRN conditional KO mice had normal myeloid lineage cell development in bone marrow, including macrophages, neutrophils, eosinophils, and dendritic cells (Supporting Information Fig. S14). Next, we explored the role of myeloid-derived PGRN in a mouse model of APAP-induced ALI (Fig. 5I). In agreement with the observation in PGRN KO mice, the survival of $PGRN^{f/f}Cre^{+}$ mice was significantly increased compared with $PGRN^{f/f}Cre^{-}$ mice after APAP overdose (Fig. 5J). $PGRN^{f/f}Cre^{+}$ developed less liver injury (Fig. 5K), evident by decreased levels of ALT and AST, as well as less expansive areas of necrosis (Fig. 5L). Compared with $PGRN^{f/f}Cre^{-}$ mice, $PGRN^{f/f}Cre^{+}$ mice had significantly more eosinophils in the liver after APAP challenge (Fig. 5M), which was associated with increased levels of IL-33, IL-4 and IL-13 (Fig. 5N). However, $PGRN^{f/f}Cre^{+}$ mice displayed a significantly decreased number of $CD11b^{+}$ $Ly6G^{+}$ neutrophils compared with $PGRN^{f/f}Cre^{-}$ mice after APAP administration. But it also did not affect the number of hepatic $CD11b^{+}F4/80^{+}$ macrophages (Supporting Information Fig. S15).

into the irradiated recipient mice separately. Eight weeks later, mice were i.p. injected with APAP. Survival rate of these mice at 0, 12, 24, 36, 48, 60, and 72 h after APAP treatment was monitored (APAP = 600 mg/kg, $n = 15$ independent biological replicates per group). (G) Serum ALT and AST levels of these mice at 24 h after APAP treatment ($n = 5$ independent biological replicates per group). (H) $Grn^{flox/flox}$ mice were generated using the CRISPR-Cas9 system. *Lyz2*-Cre^{+}-$Grn^{flox/flox}$ ($PGRN^{f/f}$ Cre^{+} mice) mice were generated by crossing the *Lyz2*-Cre^{+} mice with $Grn^{flox/flox}$ mice for specific deletion of PGRN in myeloid cells, and their *Lyz2*-Cre^{-}-$Grn^{flox/flox}$ ($PGRN^{f/f}$ Cre^{-} mice) littermates were used as controls. Image created with BioRender.com. (I) Schematic diagram of an APAP-induced ALI model in $PGRN^{f/f}$ Cre^{+} and $PGRN^{f/f}$ Cre^{-} mice. Image created with BioRender.com. (J) Survival rate of $PGRN^{f/f}$ Cre^{+} and $PGRN^{f/f}$ Cre^{-} mice at 0, 12, 24, 36, 48, 60, and 72 h after APAP treatment (APAP = 600 mg/kg, $n = 15$ independent biological replicates per group). (K) Serum ALT and AST levels of $PGRN^{f/f}$ Cre^{+} and $PGRN^{f/f}$ Cre^{-} mice at 24 h after APAP treatment ($n = 6$ independent biological replicates per group). (L) Liver necrosis was evaluated and quantified at 24 h after APAP treatment ($n = 6$ independent biological replicates per group; scale bar, 500 μm). (M) Flow cytometric analysis and the corresponding quantification of the percentages of eosinophils in hepatic $CD45^{+}$ cells at 24 h after APAP treatment ($n = 6$ independent biological replicates per group). (N) The levels of IL-33, IL-4, and IL-13 in serum and liver tissues 24 h after APAP treatment were determined by ELISA ($n = 6$ independent biological replicates per group). All data are representative of triplicate independent experiments. Data are presented as mean ± SD. $^{*}P < 0.05$, $^{**}P < 0.01$, $^{***}P < 0.001$, $^{****}P < 0.0001$ *versus* the indicated groups. *P* values were calculated based on log-rank test, one-way ANOVA, or two-tailed unpaired Student's *t*-test.

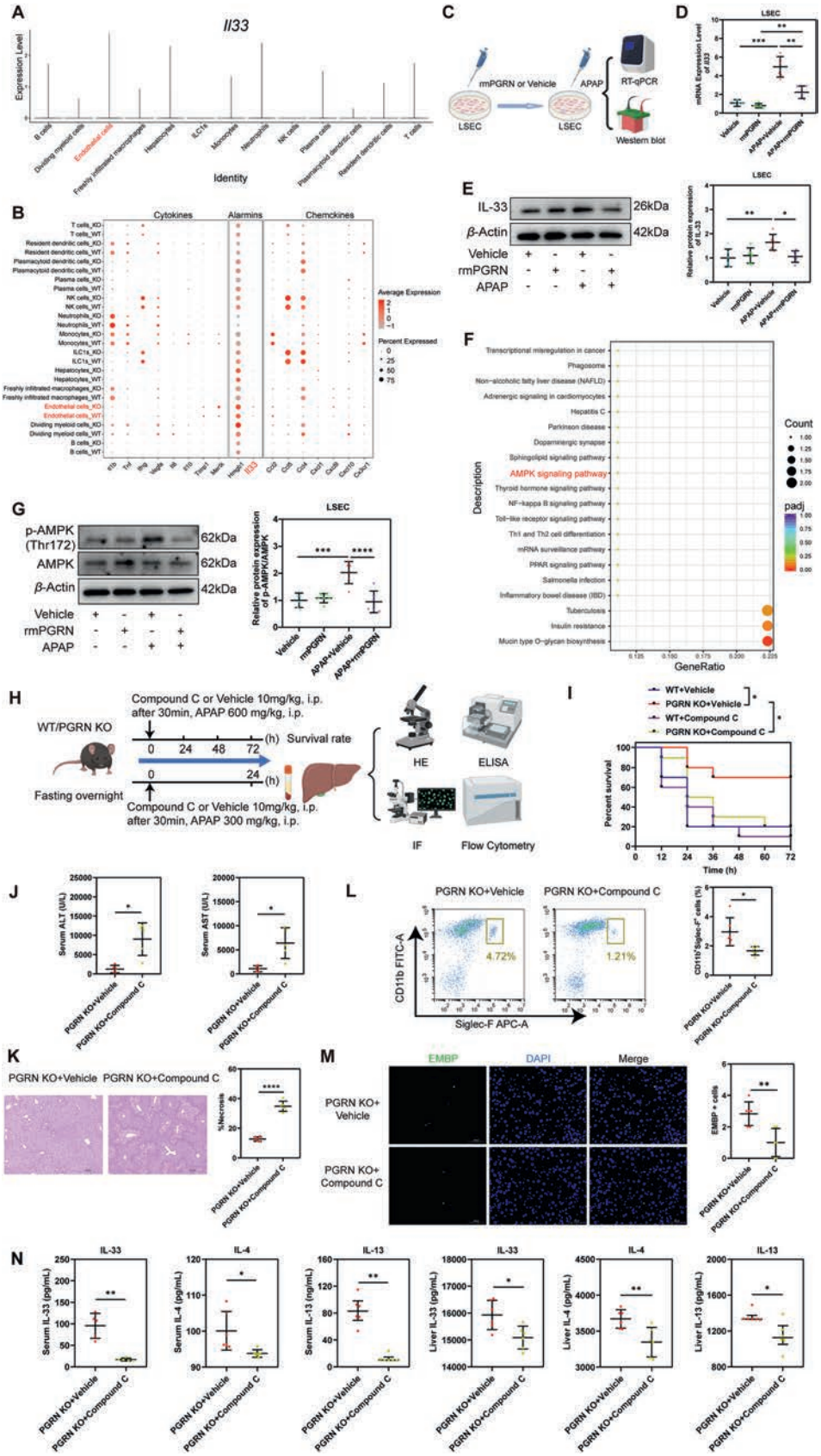

Figure 6 PGRN negatively regulates APAP-induced IL-33 expression in murine liver sinusoidal endothelial cells (LSECs) through inhibiting AMP-activated protein kinase (AMPK) signaling. (A) Violin plots show *Il33* levels in each cell type. (B) The dot plot displays the expression levels of cytokines, alarmin proteins, and chemokines in each cell type of PGRN KO mice and WT littermates after APAP treatment. (C) Primary

3.8. PGRN negatively regulates APAP-induced IL-33 expression in murine LSECs through inhibiting AMPK signaling

Having identified that LSECs were more likely the cellular source of IL-33 using PGRN KO mice and WT littermates after APAP overdose by scRNA-seq (Fig. 6A and B, Supporting Information Fig. S16). Our qPCR results also confirmed the source of IL-33 (Supporting Information Fig. S17), which is consistent with a previous work showing that IL-33 was selectively released from LSECs during APAP-induced liver injury[39]. We sought to determine whether PGRN negatively regulates IL-33 expression in LSECs to inhibit hepatic eosinophil recruitment. To test this hypothesis, primary murine LSECs ($CD45^{-}CD146^{+}$) were isolated and cultured (Supporting Information Fig. S18A−S18C), and murine LSECs were then challenged with APAP in the presence or absence of rmPGRN (Fig. 6C). rmPGRN treatment could significantly suppress APAP-induced *Il33* mRNA expression (Fig. 6D) and its protein expression in murine LSECs (Fig. 6E).

To explore the molecular mechanism by which PGRN inhibits the expression of IL-33 in LSECs, we conducted KEGG pathway evaluation on the differentially expressed genes of LSECs using scRNA-seq data. Compared with WT littermates, the activation of the AMPK signaling pathway in the LSECs of PGRN KO mice was enhanced (Fig. 6F). *In vitro* study confirmed that rmPGRN could completely inhibit APAP-induced phosphorylation of AMPK in murine LSECs (Fig. 6G).

To further examine the hepatoprotection in PGRN KO mice upon APAP overdose is due to the activation of AMPK, we treated PGRN KO mice with an inhibitor of AMPK, Compound C (Fig. 6H). Compared with vehicle control, Compound C significantly decreased the survival rate of PGRN KO mice, but not of WT littermates after APAP overdose (Fig. 6I). PGRN KO mice treated with Compound C developed much more severe liver injury, evident by an increased elevation of ALT and AST (Fig. 6J), as well as more expansive areas of necrosis (Fig. 6K). Furthermore, Compound C reduced hepatic infiltration of eosinophils in PGRN KO mice after APAP challenge (Fig. 6L and M), which was associated with significantly lower levels of IL-33, IL-4, and IL-13 (Fig. 6N). Together, results demonstrate that PGRN plays a detrimental role in APAP-induced ALI by reducing IL-33-mediated eosinophil infiltration through the suppression of AMPK activation.

3.9. AMPK and FOXO3 are involved in the downstream of PGRN modulation of APAP-induced IL-33 expression in human LSECs

To test the relevance of our results in mice to humans, we treated human LSECs (SK-Hep1 cells) with rhPGRN upon APAP challenge (Fig. 7A). As observed in murine LSECs, rhPGRN significantly inhibited APAP-induced *Il33* mRNA expression (Fig. 7B), IL-33 protein induction, and AMPK phosphorylation in human LSECs (Fig. 7C). To restore AMPK activation using an AMPK agonist (AICAR), we found that AMPK reactivation could rescue rhPGRN-impaired IL-33 expression in human LSECs (Fig. 7D and E).

To explore the mechanism underlying PGRN-mediated IL-33 down-regulation through AMPK in human LSECs, we focused on transcription factors that regulate IL-33 expression, and 20 transcription factors were identified by utilizing transcription factor databases including GTRD, KnockTF2.0, hTFtarget, and HumanTFDB (Supporting Information Fig. S19A). Subsequently, the top 20 proteins interacting with AMPK were screened using the STRING database, and protein−protein interaction (PPI) network analysis was conducted (Fig. S19B). The intersection of the two sets was taken, revealing only one transcription factor, *Foxo3* (Fig. S19C). KnockTF database showed that *Foxo3* silencing leads to a decrease in *Il33*, indicating that *Foxo3* may transcriptionally activate *Il33*. By analyzing the promoter of the human *Il33* gene using the JASPAR database, five possible binding sites for the transcription factor *Foxo3* on the *Il33* promoter were predicted. ChIP assay confirmed that *Foxo3* could directly bind to the promoter region of *Il33* (Fig. S19D−S19G), and a dual-luciferase reporter assay using truncated constructs of the *Il33* promoter further showed that *Foxo3* might bind to the *Il33* promoter and increase the luciferase activity driven by the *Il33* promoter (Fig. S19H), indicating that *Foxo3* may positively regulate the transcriptional expression of *Il33*. Similarly, our liver tissue CHIP experiment also confirmed that *Foxo3* can directly bind to the promoter region of *Il33* (Fig. S19I−S19K), strengthening the physiological relevance of our results. In fact, it has been shown that *Foxo3* dominated *Il33* expression[41], and AMPK could phosphorylate FOXO3[42,43]. We thus hypothesize that PGRN may inhibit *Il33* transcription by suppressing the AMPK−FOXO3

LSECs were cultured for 24 h, and then treated with rmPGRN (200 ng/mL) and APAP (5 mmol/L) for 24 h. Image created with BioRender.com. (D) Relative mRNA levels of *Il33* in LSECs at 24 h after APAP treatment ($n = 6$ independent biological replicates per group). (E) Western blot and densitometry analysis of IL-33 in LSECs at 24 h after APAP treatment ($n = 6$ independent biological replicates per group). (F) KEGG enrichment analysis of the top 20 upregulated genes in LSECs from PGRN KO mice compared with those from WT littermates after APAP treatment. (G) Western blot and densitometry analysis of AMPK signaling pathway in LSECs with or without APAP treatment ($n = 6$ independent biological replicates per group). (H) Schematic diagram of AMPK inhibitor (Compound C) administration in PGRN KO mice and WT littermates in the presence or absence of APAP overdose. Image created with BioRender.com. (I) Survival rate of PGRN KO mice and WT littermates at 0, 12, 24, 36, 48, 60, and 72 h after APAP treatment (APAP = 600 mg/kg, $n = 15$ independent biological replicates per group). (J) Serum concentrations of ALT and AST in PGRN KO mice treated with or without Compound C at 24 h after APAP treatment ($n = 5$ independent biological replicates per group). (K) Liver necrosis was evaluated and quantified at 24 h after APAP treatment ($n = 6$ independent biological replicates per group; scale bar, 500 μm). (L) Flow cytometric analysis images and the corresponding quantification of the percentages of eosinophils in hepatic $CD45^{+}$ cells at 24 h after APAP treatment ($n = 6$ independent biological replicates per group). (M) Immunofluorescence staining of EMBP (green) and DAPI (blue) in liver tissue and the quantification of the percentage of $EMBP^{+}$ cells at 24 h after APAP treatment ($n = 6$ independent biological replicates per group; scale bar, 50 μm). (N) The levels of IL-33, IL-4, and IL-13 in serum and liver tissues at 24 h after APAP treatment were determined by ELISA ($n = 5$−6 independent biological replicates per group). All data are representative of triplicate independent experiments. Data are presented as mean ± SD. $^{*}P < 0.05$, $^{**}P < 0.01$, $^{***}P < 0.001$, $^{****}P < 0.0001$ *versus* the indicated groups. *P* values were calculated based on one-way ANOVA, log-rank test, or two-tailed unpaired Student's *t*-test.

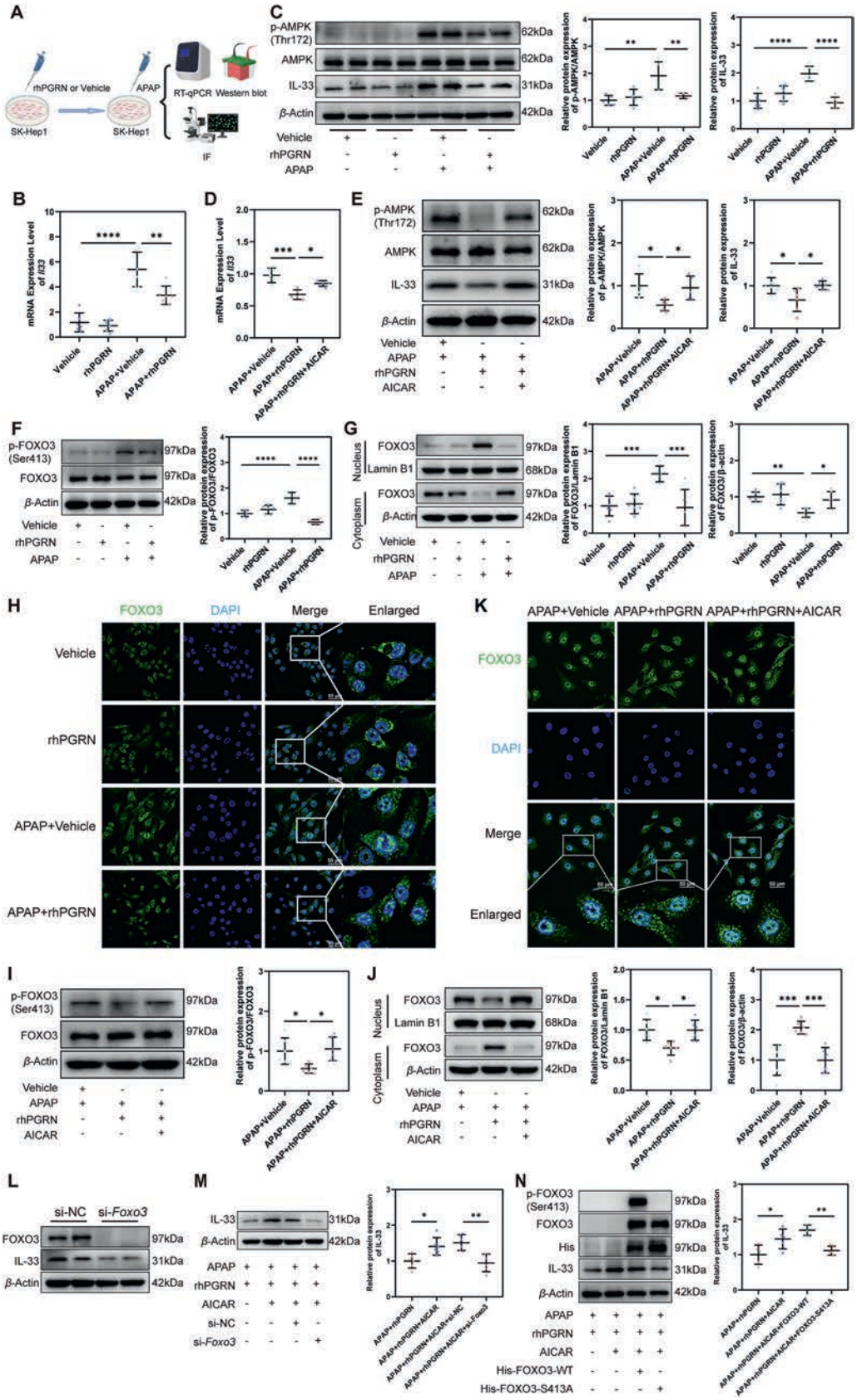

Figure 7 AMPK and forkhead box O3 (FOXO3) are involved in the downstream of PGRN modulation of APAP-induced IL-33 expression in human LSECs. (A) Human LSECs (SK-Hep1) were treated with or without rhPGRN (200 ng/mL) in the presence or absence of APAP (5 mmol/L) for 24 h, and human LSECs were then harvested for analysis. Image created with BioRender.com. (B) Relative mRNA levels of *Il33* in human

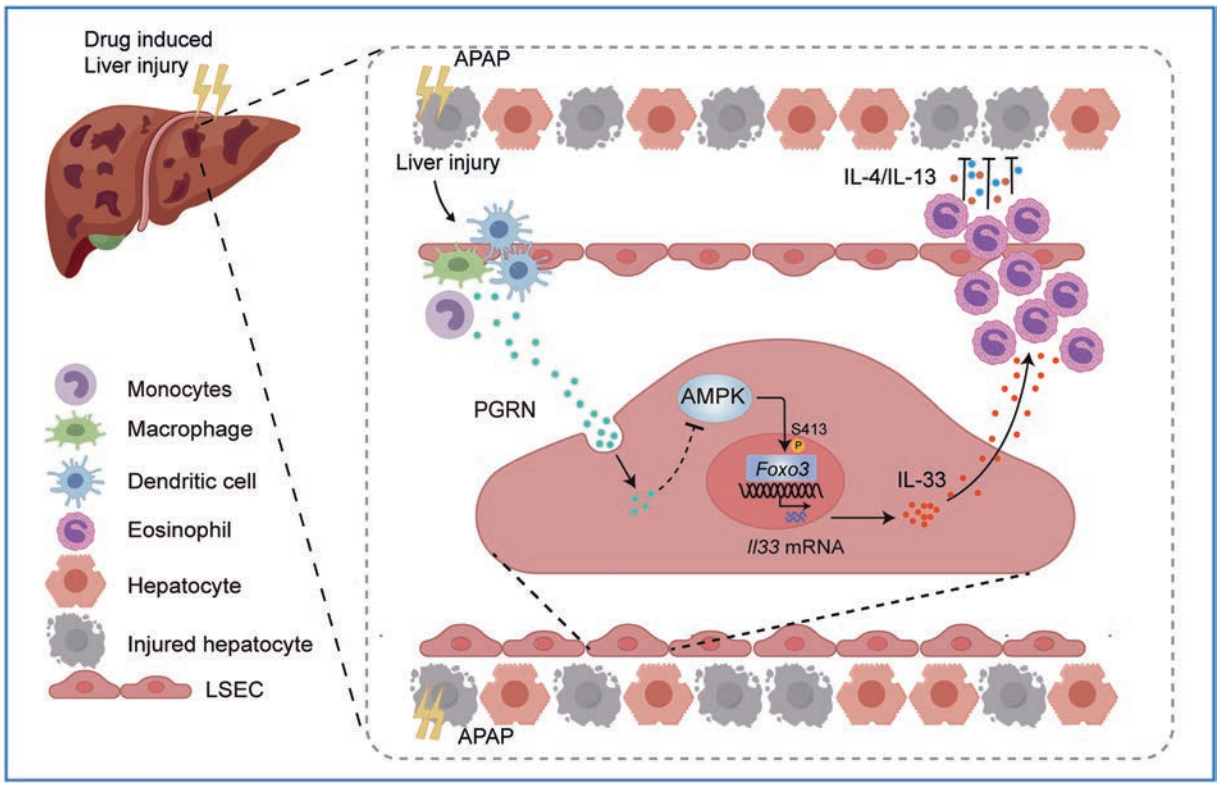

Figure 8 Schematic summary of the main findings. Upon APAP overdose, the hepatic levels of PGRN secreted by myeloid cells, including monocytes, macrophages, and dendritic cells, are elevated. In LSECs, the major cellular source of IL-33 during APAP-induced ALI, PGRN suppresses AMPK activation and inhibits the nuclear translocation of the transcription factor *Foxo3*, thereby down-regulating IL-33 expression in LSECs. The resulting decrease in IL-33 expression reduces eosinophil recruitment, which subsequently diminishes IL-4 and IL-13 secretion, leading to impairment of protective function in eosinophils and culminating in APAP-induced liver failure. Image created with Figdraw.com.

signaling in human LSECs. As expected, rhPGRN inhibited APAP-induced phosphorylation and nuclear translocation of FOXO3 in human LSECs (Fig. 7F−H), and AMPK activation by AICAR could reverse rhPGRN-impaired phosphorylation and nuclear translocation of FOXO3 in human LSECs after APAP treatment (Fig. 7I−K). Furthermore, knockdown of *Foxo3* in human LSECs by siRNA could inhibit AICAR-induced increase of IL-33 expression in the presence of rhPGRN after APAP treatment (Fig. 7L and M). We also found that AMPK mainly phosphorylates FOXO3 at the S413 site. To confirm this result, we constructed an S413A mutant plasmid. As expected, AMPK activation by AICAR phosphorylated FOXO3-WT, but did not phosphorylate the S413A mutant. Meanwhile, the S413A mutation led to a decrease in the expression of IL-33 (Fig. 7N). Taken together, PGRN promoted APAP-induced ALI by impairing hepatic recruitment of eosinophils through inhibiting IL-33 expression in LSECs, which was dependent on the disruption of the AMPK−FOXO3 signaling pathway (Fig. 8).

LSECs ($n = 6$ independent biological replicates per group). (C) Western blot and densitometry analysis of AMPK signaling pathway and IL-33 in human LSECs ($n = 6$ independent biological replicates per group). (D) Human LSECs were treated with AICAR (200 μmol/L), rhPGRN (200 ng/mL), and APAP (5 mmol/L) for 24 h. Relative mRNA levels of *Il33* expression were detected by qPCR ($n = 5$ independent biological replicates per group). (E) Western blot and densitometry analysis of AMPK phosphorylation and IL-33 protein levels in human LSECs ($n = 5$−6 independent biological replicates per group). (F) Western blot and densitometry analysis of FOXO3 phosphorylation in human LSECs ($n = 6$ independent biological replicates per group). (G) Western blot and densitometry analysis of plasma protein and nucleoprotein of FOXO3 in human LSECs ($n = 6$ independent biological replicates per group). (H) Immunofluorescence staining of FOXO3 (green) and 4′,6-diamidino-2-phenylindole (DAPI, blue) in human LSECs (scale bar, 50 μm). (I) Western blot and densitometry analysis of FOXO3 phosphorylation in human LSECs ($n = 6$ independent biological replicates per group). (J) Western blot and densitometry analysis of the cytoplasmic and nuclear protein fractions of FOXO3 in human LSECs ($n = 6$ independent biological replicates per group). (K) Immunofluorescence staining of FOXO3 (green) and DAPI (blue) in human LSECs (scale bar, 50 μm). (L) Human LSECs were transfected with either negative control siRNA (si-NC) or *Foxo3* siRNA (si-*Foxo3*) for 24 h. The expression levels of FOXO3 and IL-33 in human LSECs were measured by Western blot. (M) Western blot and densitometry analysis of IL-33 protein expression in human LSECs treated with or without AICAR ($n = 6$ independent biological replicates per group). (N) Human LSECs were transfected with either FOXO3-WT or FOXO3-S413A for 24 h. Western blot and densitometry analysis of IL-33 protein expression in human LSECs treated with or without AICAR ($n = 5$ independent biological replicates per group). Data are representative of triplicate independent experiments. Data are presented as mean ± SD. $^{*}P < 0.05$, $^{**}P < 0.01$, $^{***}P < 0.001$, $^{****}P < 0.0001$ *versus* the indicated groups. *P* values were calculated based on one-way ANOVA.

4. Discussion

Due to the high disease-related mortality and limited treatment options, DILI, especially APAP-induced ALI, remains an urgent and inadequately addressed clinical problem. Our study uncovers a disease mechanism that contributes to the pathogenesis of APAP-induced ALI and ConA-induced liver toxicity. We identify myeloid-derived PGRN as a disease-promoting mediator that can be inhibited to protect against lethal APAP-induced ALI in the mouse model. These findings are of immediate importance to our understanding of the pathogenesis of liver injury caused by APAP overdose and may open new avenues for its treatment.

PGRN has been well established as a key multifunctional regulator of tissue injury and inflammation[10,11]. A role for PGRN in the manifestation of DILI remains unresolved, and controversy exists regarding the contribution of PGRN to liver diseases[8-11]. A previous study has shown that PGRN expression contributed to the malignancy of hepatocellular carcinoma cells[44]. Following lymphocytic choriomeningitis virus infection, the absence of PGRN in mice culminated in increased liver immunopathology[45]. In the CCl4-induced fibrosis mouse model, PGRN showed protective effects against hepatic injury[21]. Here, we used multiple approaches to demonstrate that PGRN could drive the development of APAP-induced ALI. Mice with global deletion or myeloid cell-specific conditional knockout of PGRN were refractory to APAP overdose. rmPGRN supplementation could exaggerate APAP-induced ALI, while blocking PGRN induction with its antibody protected mice from APAP challenge. Therefore, we provided the first direct functional evidence linking PGRN to APAP-induced ALI, which documents the potential of PGRN inhibition as a potential approach to treat APAP overdose-induced ALI.

Our finding that PGRN deficiency is protective in APAP-induced ALI appears to contrast with its reported protective roles in models of liver fibrosis. This underscores the context-dependent effects of PGRN in liver pathophysiology. Here, PGRN appears to function as a brake on an early reparative immune response, thereby exacerbating injury. In chronic inflammatory and fibrotic diseases, the disease milieu is dominated by persistent inflammation, macrophage activation, and activation of hepatic stellate cells. In these settings, PGRN is often reported to exert anti-inflammatory effects and direct anti-fibrotic actions[21]. Therefore, the effect of PGRN likely depends on the predominant pathological process and the specific cellular targets available in a given disease context. In APAP toxicity, its suppressive effect on a rapid innate repair pathway prevails. In contrast, in chronic settings, its beneficial modulation of sustained inflammation and fibrosis becomes the dominant and protective function. This dual nature highlights the complexity of PGRN biology and emphasizes that therapeutic targeting of PGRN would require careful consideration of the specific disease etiology.

Our study identified eosinophils as a key defense mechanism regulated by PGRN and demonstrated that the enhanced hepatic recruitment of eosinophils mediated the protective effect of PGRN removal on APAP overdose. In mice treated with APAP, CCl4, or ConA, as well as mice with hepatic ischemia−reperfusion injury, eosinophils were recruited into the liver and played a profound protective role[39,40]. Mice deficient of IL-33 exhibited impaired hepatic eosinophil recruitment[40], indicating that IL-33 is a critical upstream cytokine mediating hepatic recruitment of eosinophils and their protective function in APAP-induced ALI. Furthermore, IL-33 stimulation of eosinophils protected against APAP-induced liver injury through IL-4 and IL-13 production. During APAP-induced ALI, IL-33 has been reported to be selectively released from LSECs[39]. Our studies found that IL-33-dependent hepatic recruitment of eosinophils in PGRN KO mice after APAP overdose was significantly elevated, and both scRNA-seq and flow cytometry analysis unequivocally identified LSECs as the main source of IL-33 after APAP challenge. These data highlight the importance of PGRN-mediated crosstalk between eosinophils and LSECs, *via* IL-33 plays an important role in eosinophil recruitment to the APAP-injured liver. A key study demonstrates that IL-33 levels are significantly elevated as early as 6 h post-APAP[46]. Furthermore, eosinophil influx begins by 8 h, and adoptive transfer experiments confirm their functional protection at this time[39]. Given that PGRN deficiency does not alter the initial metabolic phase of APAP injury. This effectively rules out altered APAP bioactivation as the cause of protection, consistent with reports of other immunomodulatory proteins that confer protection without affecting early metabolism[25,47]. We observed the absence of protective effects of PGRN in our APAP modeling system at 6 h; this observation might be linked to the rapid activation of the IL-33−eosinophil axis. However, PGRN up-regulated IL-33 production in airway epithelial cells[48].

On the molecular mechanisms by which PGRN negatively regulated APAP-induced IL-33 production in LSECs, we found that the increased expression of PGRN was accompanied by the suppression of the AMPK signaling pathway in LSECs, which is consistent with previous reports showing that AMPK activation exhibited protective effects on APAP-induced liver failure[23,49,50]. PGRN has been shown to attenuate high-glucose-induced podocyte injury by activating AMPK[51], and PGRN could alleviate the mitochondrial damage during regulatory T cells differentiation by activating AMPK[52]. However, the suppression effects of PGRN on AMPK activation remain unknown. By using both genetic tools and pharmacological compounds, we consistently documented the significance of the AMPK signaling pathway in IL-33 expression and eosinophil recruitment negatively regulated by PGRN upon APAP challenge. *Foxo3*, a transcription factor directly regulated by AMPK, is a key player in the regulation of liver injury[53-55]. Our ChIP and dual-luciferase reporter assays confirmed that *Foxo3*, acting as a transcriptional activator, could bind to the *Il33* promoter region and induce its transcription. Further experiments revealed that PGRN prevented APAP-induced phosphorylation and nuclear translocation of FOXO3 by suppressing AMPK activation, leading to a significant decrease in IL-33 production from LSECs. These findings uncovered a previously unrecognized molecular mechanism involved in PGRN-dependent IL-33 expression in mediating hepatoprotective function of eosinophils *via* the AMPK−FOXO3 signaling pathway.

Patients with APAP-induced ALI are more likely to die while on the liver transplant waiting list than those with other causes of acute liver failure[56,57]. An important strength of this study is that we reported increased PGRN levels in peripheral blood in human patients suffering from APAP overdose, and patients with higher serum PGRN levels experienced more severe liver injury. Therefore, PGRN might be considered as an additional biomarker of APAP overdose. In our study, blocking PGRN elevation with its antibody not only reduced liver injury but also improved survival after APAP-induced ALI in WT mice, which suggests an immediate translational ramification. Therefore, after identifying patients with APAP overdose at high risk of liver failure based on serum PGRN levels, it is possible to reduce the risk of severe liver injury. However, the kinetics of PGRN release are not well understood in patients with APAP overdose; hence, further clinical

trials are required to elucidate the therapeutic value of the blockade of circulating PGRN against APAP-induced ALI.

In summary, we have presented data in mice and humans demonstrating that PGRN promoted APAP-induced hepatotoxicity through the impairment of hepatic recruitment of eosinophils by decreasing IL-33 expression in LSECs, which was dependent on the suppression of the AMPK−FOXO3 signaling pathway. Therefore, a possible theranostic approach involving blood-circulating PGRN guided patient identification and targeted therapy antagonizing PGRN activity may help improve the management of APAP-induced ALI or other ALI. These findings obtained from APAP-challenged mice still need to be confirmed in a clinical context.

Our research also has some limitations. First, our research focused on eosinophils, but NKT cells or ILC2 cells can also respond to IL-33[58-60]. Exploring whether these cell types may be influenced by PGRN deficiency would further enhance mechanistic depth. Second, *Lyz2-Cre* is expressed in a broad range of myeloid cells, including monocytes, macrophages, and neutrophils. Therefore, our data from *Lyz2-Cre* knockout models definitively demonstrate that hematopoietic-derived myeloid cells are a major source of functionally relevant PGRN, but they cannot distinguish the relative contributions of specific myeloid subsets. So, we will use cell-type-specific knockout mice to dissect the role of each myeloid subset in detail. Third, how PGRN will affect the LSECs is unknown. Due to the many receptors for PGRN[8], no specific research and discussion were carried out in our research, which is also a limitation of ours. In subsequent work, we will also discuss this direction.

5. Conclusions

In this study, we found that serum PGRN levels are increased and positively correlated with the severity of liver injury and may serve as a potential biomarker for APAP-induced ALI. Mice deficient in PGRN are refractory to APAP-induced ALI, which is dependent on the increase of IL-33-mediated hepatic recruitment of eosinophils and their protective function. PGRN inhibits hepatic recruitment of eosinophils by dampening APAP-induced IL-33 expression in liver sinusoidal endothelial cells through the suppression of AMPK−FOXO3 signaling pathway activation. A potential theranostic approach involving blood-circulating PGRN guided patient identification and targeted therapy antagonizing PGRN activity may help improve the management of APAP-induced ALI.

Acknowledgments

This work was supported by the National Natural Science Foundation of China (Grant Nos. 82530074 and 82370009), Natural Science Foundation Project of Chongqing (CSTB2022NSCQ-LZX0017, China), and Chongqing Medical Scientific Research Project (Joint Project of Chongqing Health Commission and Science and Technology Bureau (2024ZDXM002, China)).

Author contributions

Conceptualization: Yin Tang, Ju Cao; Methodology: Yin Tang, Siyuan Xie, Yueyue He; Formal analysis: Yin Tang, Siyuan Xie, Yueyue He; Investigation: Jiayu Liu, Mingang Pan, Renlin Yu, Linghong Zhou, Mengxue Liu, Yi Liu; Data curation: Yi Liu, Ju Cao; Writing - original draft: Yin Tang, Siyuan Xie; Writing - review & editing: Yin Tang, Ju Cao; Visualization: Mingang Pan; Supervision: Ju Cao; Project administration: Yi Liu, Ju Cao; Funding acquisition: Ju Cao. Yin Tang, Siyuan Xie, and Yueyue He contributed equally to this work.

Conflicts of interest

The authors declare no conflicts of interest.

Data availability

RNA-seq data are available at GEO under accession numbers GSE305178 and GSE305180. scRNA-seq data are available at GEO under accession number GSE305873. All data relevant to the study are included in the article or uploaded as Supporting Information Further information may be provided upon reasonable request to the corresponding author.

Appendix A. Supporting information

Supporting information to this article can be found online at https://doi.org/10.1016/j.apsb.2026.02.011.

References

1. Lucena MI, Sanabria J, García-Cortes M, Stephens C, Andrade RJ. Drug-induced liver injury in older people. *Lancet Gastroenterol Hepatol* 2020;**5**:862−74.
2. Hoofnagle JH, Björnsson ES. Drug-induced liver injury—types and phenotypes. *N Engl J Med* 2019;**381**:264−73.
3. Lee WM. Acetaminophen and the U.S. acute liver failure study group: lowering the risks of hepatic failure. *Hepatology* 2004;**40**:6−9.
4. Woolbright BL, Jaeschke H. Role of the inflammasome in acetaminophen-induced liver injury and acute liver failure. *J Hepatol* 2017;**66**:836−48.
5. Jaeschke H, Ramachandran A. Acetaminophen hepatotoxicity: paradigm for understanding mechanisms of drug-induced liver injury. *Annu Rev Pathol* 2024;**19**:453−78.
6. Woolbright BL, Jaeschke H. Mechanisms of inflammatory liver injury and drug-induced hepatotoxicity. *Curr Pharmacol Rep* 2018;**4**: 346−57.
7. Bhushan B, Apte U. Liver regeneration after acetaminophen hepatotoxicity: mechanisms and therapeutic opportunities. *Am J Pathol* 2019; **189**:719−29.
8. Huang G, Jian J, Liu CJ. Progranulinopathy: a diverse realm of disorders linked to progranulin imbalances. *Cytokine Growth Factor Rev* 2024;**76**:142−59.
9. Rhinn H, Tatton N, McCaughey S, Kurnellas M, Rosenthal A. Progranulin as a therapeutic target in neurodegenerative diseases. *Trends Pharmacol Sci* 2022;**43**:641−52.
10. Lan YJ, Sam NB, Cheng MH, Pan HF, Gao J. Progranulin as a potential therapeutic target in immune-mediated diseases. *J Inflamm Res* 2021;**14**:6543−56.
11. Cui Y, Hettinghouse A, Liu CJ. Progranulin: a conductor of receptors orchestra, a chaperone of lysosomal enzymes and a therapeutic target for multiple diseases. *Cytokine Growth Factor Rev* 2019;**45**:53−64.
12. Liu J, Li Y, Liu Y, Yu R, Yin Y, Lai X, et al. Elevated serum level of progranulin is associated with increased mortality in critically ill patients with candidemia. *Microb Infect* 2024;**26**:105302.
13. Luo Q, Yan X, Tu H, Yin Y, Cao J. Progranulin aggravates pulmonary immunopathology during influenza virus infection. *Thorax* 2019;**74**: 305−8.

14. Liu J, Lai X, Yu R, Ding H, Bai H, Yang Z, et al. Progranulin aggravates lethal *Candida albicans* sepsis by regulating inflammatory response and antifungal immunity. *PLoS Pathog* 2022;**18**:e1010873.
15. Song Z, Zhang X, Zhang L, Xu F, Tao X, Zhang H, et al. Progranulin plays a central role in host defense during sepsis by promoting macrophage recruitment. *Am J Respir Crit Care Med* 2016;**194**: 1219−32.
16. Zou S, Luo Q, Song Z, Zhang L, Xia Y, Xu H, et al. Contribution of progranulin to protective lung immunity during bacterial pneumonia. *J Infect Dis* 2017;**215**:1764−73.
17. Huang J, Liu B, Liu Y, You W, Zhao P, Liu Y, et al. Progranulin protects against *Clostridioides difficile* infection by enhancing IL-22 production. *Gut Microbes* 2024;**16**:2409220.
18. Yang F, Cheng MH, Pan HF, Gao J. Progranulin: a promising biomarker and therapeutic target for fibrotic diseases. *Acta Pharm Sin B* 2024;**14**:3312−26.
19. Astuti Y, Raymant M, Quaranta V, Clarke K, Abudula M, Smith O, et al. Efferocytosis reprograms the tumor microenvironment to promote pancreatic cancer liver metastasis. *Nat Cancer* 2024;**5**:774−90.
20. Yilmaz Y, Eren F, Yonal O, Polat Z, Bacha M, Kurt R, et al. Serum progranulin as an independent marker of liver fibrosis in patients with biopsy-proven nonalcoholic fatty liver disease. *Dis Markers* 2011;**31**: 205−10.
21. Yoo W, Lee J, Noh KH, Lee S, Jung D, Kabir MH, et al. Progranulin attenuates liver fibrosis by downregulating the inflammatory response. *Cell Death Dis* 2019;**10**:758.
22. Zheng S, Li Z, Song J, Wang P, Xu J, Hu W, et al. Endothelial metrnl determines circulating metrnl level and maintains endothelial function against atherosclerosis. *Acta Pharm Sin B* 2023;**13**:1568−87.
23. Lin Z, Wu F, Lin S, Pan X, Jin L, Lu T, et al. Adiponectin protects against acetaminophen-induced mitochondrial dysfunction and acute liver injury by promoting autophagy in mice. *J Hepatol* 2014;**61**:825−31.
24. Han Y, Black S, Gong Z, Chen Z, Ko JK, Zhou Z, et al. Membrane-delimited signaling and cytosolic action of MG53 preserve hepatocyte integrity during drug-induced liver injury. *J Hepatol* 2022;**76**:558−67.
25. Li M, Sun X, Zhao J, Xia L, Li J, Xu M, et al. CCL5 deficiency promotes liver repair by improving inflammation resolution and liver regeneration through M2 macrophage polarization. *Cell Mol Immunol* 2020;**17**:753−64.
26. Abdelmegeed MA, Banerjee A, Yoo SH, Jang S, Gonzalez FJ, Song BJ. Critical role of cytochrome P450 2E1 (CYP2E1) in the development of high fat-induced non-alcoholic steatohepatitis. *J Hepatol* 2012;**57**:860−6.
27. Wen Y, Wang C, Gu J, Yu C, Wang K, Sun X, et al. Metabolic modulation of acetaminophen-induced hepatotoxicity by osteopontin. *Cell Mol Immunol* 2019;**16**:483−94.
28. Tan W, Liu J, Yu R, Zhao P, Liu Y, Lu Q, et al. Trim72 is a major host factor protecting against lethal *Candida albicans* infection. *PLoS Pathog* 2024;**20**:e1012747.
29. Bai H, Lu Q, Wu C, Xu F, Liu J, Wang K, et al. Bone morphogenetic protein 9 is a candidate prognostic biomarker and host-directed therapy target for sepsis. *Sci Transl Med* 2024;**16**:eadi3275.
30. Linke A, Cicek H, Müller A, Meyer-Schwesinger C, Melderis S, Wiech T, et al. Antigen cross-presentation by murine proximal tubular epithelial cells induces cytotoxic and inflammatory $CD8^+$ T cells. *Cells* 2022;**11**:1510.
31. Mierzejewski B, Grabowska I, Jackowski D, Irhashava A, Michalska Z, Stremińska W, et al. Mouse $CD146^+$ muscle interstitial progenitor cells differ from satellite cells and present myogenic potential. *Stem Cell Res Ther* 2020;**11**:341.
32. Badmann A, Langsch S, Keogh A, Brunner T, Kaufmann T, Corazza N. TRAIL enhances paracetamol-induced liver sinusoidal endothelial cell death in a Bim- and Bid-dependent manner. *Cell Death Dis* 2012;**3**:e447.
33. Xiang S, Wang Y, Lei D, Luo Y, Peng D, Zong K, et al. Donor graft METTL3 gene transfer ameliorates rat liver transplantation ischemia−reperfusion injury by enhancing HO-1 expression in an m^6A-dependent manner. *Clin Immunol* 2023;**251**:109325.
34. Lei D, Wang Y, Li S, Xiang S, Luo Y, Yan P, et al. MAFF alleviates hepatic ischemia−reperfusion injury by regulating the CLCF1/STAT3 signaling pathway. *Cell Mol Biol Lett* 2025;**30**:39.
35. Wang L, Feng Y, Xie X, Wu H, Su XN, Qi J, et al. Neuropilin-1 aggravates liver cirrhosis by promoting angiogenesis *via* VEGFR2-dependent PI3K/Akt pathway in hepatic sinusoidal endothelial cells. *EBioMedicine* 2019;**43**:525−36.
36. Triantafyllou E, Pop OT, Possamai LA, Wilhelm A, Liaskou E, Singanayagam A, et al. MerTK expressing hepatic macrophages promote the resolution of inflammation in acute liver failure. *Gut* 2018;**67**:333−47.
37. Weyer K, Glerup S. Placental regulation of peptide hormone and growth factor activity by proMBP. *Biol Reprod* 2011;**84**:1077−86.
38. Wang Y, Yang Y, Wang M, Wang S, Jeong JM, Xu L, et al. Eosinophils attenuate hepatic ischemia−reperfusion injury in mice through ST2-dependent IL-13 production. *Sci Transl Med* 2021;**13**: eabb6576.
39. Xu L, Yang Y, Wen Y, Jeong JM, Emontzpohl C, Atkins CL, et al. Hepatic recruitment of eosinophils and their protective function during acute liver injury. *J Hepatol* 2022;**77**:344−52.
40. Xu L, Yang Y, Jiang J, Wen Y, Jeong JM, Emontzpohl C, et al. Eosinophils protect against acetaminophen-induced liver injury through cyclooxygenase-mediated IL-4/IL-13 production. *Hepatology* 2023; **77**:456−65.
41. Zhu D, Liu S, Huang K, Wang Z, Hu S, Li J, et al. Intrapericardial exosome therapy dampens cardiac injury *via* activating Foxo3. *Circ Res* 2022;**131**:e135−50.
42. Greer EL, Oskoui PR, Banko MR, Maniar JM, Gygi MP, Gygi SP, et al. The energy sensor AMP-activated protein kinase directly regulates the mammalian Foxo3 transcription factor. *J Biol Chem* 2007; **282**:30107−19.
43. Li XN, Song J, Zhang L, LeMaire SA, Hou X, Zhang C, et al. Activation of the AMPK−FOXO3 pathway reduces fatty acid-induced increase in intracellular reactive oxygen species by upregulating thioredoxin. *Diabetes* 2009;**58**:2246−57.
44. Liu F, Zhang W, Yang F, Feng T, Zhou M, Yu Y, et al. Interleukin-6-stimulated progranulin expression contributes to the malignancy of hepatocellular carcinoma cells by activating mTOR signaling. *Sci Rep* 2016;**6**:21260.
45. Huang A, Shinde PV, Huang J, Senff T, Xu HC, Margotta C, et al. Progranulin prevents regulatory NK cell cytotoxicity against antiviral T cells. *JCI Insight* 2019;**4**:e129856.
46. Wang Z, Wu L, Pan B, Chen Y, Zhang T, Tang N. Interleukin 33 mediates hepatocyte autophagy and innate immune response in the early phase of acetaminophen-induced acute liver injury. *Toxicology* 2021;**456**:152788.
47. Hou X, Liu Q, Gao Y, Yong L, Xie H, Li W, et al. Mesencephalic astrocyte-derived neurotrophic factor reprograms macrophages to ameliorate acetaminophen-induced acute liver injury *via* p38 MAPK pathway. *Cell Death Dis* 2022;**13**:100.
48. Choi JP, Park SY, Moon KA, Ha EH, Woo YD, Chung DH, et al. Macrophage-derived progranulin promotes allergen-induced airway inflammation. *Allergy* 2020;**75**:1133−45.
49. Lv H, Hong L, Tian Y, Yin C, Zhu C, Feng H. Corilagin alleviates acetaminophen-induced hepatotoxicity *via* enhancing the AMPK/GSK3β−Nrf2 signaling pathway. *Cell Commun Signal* 2019; **17**:2.
50. Li C, Ming Y, Wang Z, Xu Q, Yao L, Xu D, et al. GADD45α alleviates acetaminophen-induced hepatotoxicity by promoting AMPK activation. *Cell Mol Life Sci* 2019;**76**:129−45.
51. Zhou D, Zhou M, Wang Z, Fu Y, Jia M, Wang X, et al. Progranulin alleviates podocyte injury *via* regulating CAMKK/AMPK-mediated autophagy under diabetic conditions. *J Mol Med (Berl)* 2019;**97**: 1507−20.
52. Chen Y, Guo M, Xie K, Lei M, Chai Y, Zhang Z, et al. Progranulin promotes regulatory T cells plasticity by mitochondrial metabolism through AMPK/PGC-1α pathway in ARDS. *Clin Immunol* 2024;**261**: 109940.

53. Peng J, Liang G, Li Y, Mao S, Zhang C, Wang Y, et al. Identification of a novel FOXO3 agonist that protects against alcohol induced liver injury. *Biochem Biophys Res Commun* 2024;**704**:149690.
54. Omorou M, Huang Y, Gao M, Mu C, Xu W, Han Y, et al. The forkhead box O3 (FOXO3): a key player in the regulation of ischemia and reperfusion injury. *Cell Mol Life Sci* 2023;**80**:102.
55. Deng S, Cao H, Li T, Wang X, Meng J, Zeng T, et al. *Lachnospiraceae-bacterium* alleviates ischemia−reperfusion injury in steatotic donor liver by inhibiting ferroptosis *via* the Foxo3−Alox15 signaling pathway. *Gut Microbes* 2025;**17**:2460543.
56. Karvellas CJ, Leventhal TM, Rakela JL, Zhang J, Durkalski V, Reddy KR, et al. Outcomes of patients with acute liver failure listed for liver transplantation: a multicenter prospective cohort analysis. *Liver Transplant* 2023;**29**:318−30.
57. Umbaugh DS, Nguyen NT, Curry SC, Rule JA, Lee WM, Ramachandran A, et al. The chemokine CXCL14 is a novel early prognostic biomarker for poor outcome in acetaminophen-induced acute liver failure. *Hepatology* 2024;**79**:1352−64.
58. Benvie AM, Berry DC. Reversing Pdgfrβ signaling restores metabolically active beige adipocytes by alleviating ILC2 suppression in aged and obese mice. *Mol Metabol* 2024;**89**:102028.
59. Stockis J, Yip T, Moreno-Vicente J, Burton O, Samarakoon Y, Schuijs MJ, et al. Cross-talk between ILC2 and Gata3^{high} T_{regs} locally constrains adaptive type 2 immunity. *Sci Immunol* 2024;**9**:eadl1903.
60. Awada A, Nicaise C, Ena S, Schandéné L, Rasschaert J, Popescu I, et al. Potential involvement of the IL-33−ST2 axis in the pathogenesis of primary Sjogren's syndrome. *Ann Rheum Dis* 2014;**73**:1259−63.